Acoustic gas thermometry

2014 Metrologia 51 R1

(http://iopscience.iop.org/0026-1394/51/1/R1)

IOP Publishing | Bureau International des Poids et Mesures Metrologia

Metrologia **51** (2014) R1–R19 doi:10.1088/0026-1394/51/1/R1

REVIEW ARTICLE

Acoustic gas thermometry

M R Moldover[1], R M Gavioso[2], J B Mehl[3], L Pitre[4], M de Podesta[5] and J T Zhang[6]

[1] Sensor Science Division, National Institute of Standards and Technology, Gaithersburg, MD, USA
[2] Thermodynamics Division, Istituto Nazionale di Ricerca Metrologica, 10135 Turin, Italy
[3] 36 Zunuqua Trail, PO Box 307, Orcas, WA 98280-0307, USA
[4] Laboratoire Commun de Métrologie LNE-Cnam (LCM), 61 rue du Landy, 93210 La Plaine Saint-Denis, France
[5] National Physical Laboratory, Teddington, Middlesex, TW11 0LW, UK
[6] National Institute of Metrology, Beijing 100013, People's Republic of China

Received 27 July 2013, revised 7 November 2013
Accepted for publication 14 November 2013
Published 16 January 2014

Abstract

We review the principles, techniques and results from primary acoustic gas thermometry (AGT). Since the establishment of ITS-90, the International Temperature Scale of 1990, spherical and quasi-spherical cavity resonators have been used to realize primary AGT in the temperature range 7 K to 552 K. Throughout the sub-range 90 K $< T <$ 384 K, at least two laboratories measured $(T - T_{90})$. (Here T is the thermodynamic temperature and T_{90} is the temperature on ITS-90.) With a minor exception, the resulting values of $(T - T_{90})$ are mutually consistent within $3 \times 10^{-6}\, T$. These consistent measurements were obtained using helium and argon as thermometric gases inside cavities that had radii ranging from 40 mm to 90 mm and that had walls made of copper or aluminium or stainless steel. The AGT values of $(T - T_{90})$ fall on a smooth curve that is outside $\pm u(T_{90})$, the estimated uncertainty of T_{90}. Thus, the AGT results imply that ITS-90 has errors that could be reduced in a future temperature scale. Recently developed techniques imply that low-uncertainty AGT can be realized at temperatures up to 1350 K or higher and also at temperatures in the liquid-helium range.

Keywords: thermometry, thermodynamic temperature, acoustic resonators, microwave resonators, thermophysics, speed of sound, properties of gases, helium, argon, kelvin, units

(Some figures may appear in colour only in the online journal)

S Online supplementary data available from stacks.iop.org/Met/51/R1/mmedia

1. Introduction: overview AGT

'Absolute' primary, acoustic gas thermometry (AGT) determines the thermodynamic temperature T from measurements of the absolute speed of sound u in a low-density, monatomic gas with average molar mass M that are traceable to the metre, kilogram and the second. Over the past decade, the thermometry community has refined absolute AGT near the temperature of the triple point of water T_{TPW} in preparation for redefining the kelvin in terms of the Boltzmann constant. The community has achieved uncertainties of order $10^{-6}u(T, p)$ in helium and argon on isotherms near T_{TPW}. This achievement used highly specialized apparatus and gas samples that were characterized for chemical impurities and, in the case of argon, relative isotopic abundances. In contrast, 'relative' primary AGT determines the ratios of thermodynamic temperatures from measurements of the ratios of speeds of sound conducted on the isotherms of interest. Such ratio measurements are simpler than absolute measurements because they do not require traceability to either the metre or the second or the kilogram and because many instrumental uncertainties cancel out of the ratio. The ratio measurements do require measuring ratios of lengths and frequencies. They also require that the average molecular mass of the thermometric gas does not change while the speed-of-sound ratios are measured. Thus, noble gas impurities in a noble working gas are acceptable for relative

AGT conducted under conditions such that the gas mixture does not fractionate.

This review concentrates on fixed-path, gas-filled, cavity-resonator, acoustic thermometers. Since 1990, these instruments have realized relative AGT in the temperature range from 7 K to 633 K. These instruments used sophisticated design and measurement techniques to realize AGT with low uncertainties; however, each instrument generated highly redundant data. Routinely, the resonance frequencies and the resonance half-widths of several microwave and acoustic modes were measured at each value of temperature and pressure. When the apparatus was well understood, the resonance frequencies of the various modes yielded consistent speeds of sound and the half-widths of the resonances were consistent with theory. These consistency checks support the theoretically derived corrections that were applied to the raw acoustic and microwave data.

In the temperature range 90 K to 384 K at least two different laboratories used AGT to measure $(T - T_{90})$. With a minor exception, the results from the diverse laboratories are mutually consistent within $3.2 \times 10^{-6}\,T$. These remarkably consistent results were obtained using both helium and argon as thermometric gases in cavities that had radii ranging from 40 mm to 90 mm and that had walls made of either copper, aluminium, or stainless steel. As discussed in section 12, the AGT values of $(T - T_{90})$ fall on a smooth curve that is outside $\pm u(T_{90})$, the estimated uncertainty of T_{90}. The AGT results imply $(T - T_{90})/T \approx -6 \times 10^{-5}$ near 90 K and $(T - T_{90})/T \approx 2 \times 10^{-5}$ near 384 K. These errors in ITS-90 could be reduced by a factor of five or more in a future temperature scale.

In the concluding section, we identify plausible extensions of demonstrated techniques that will enable accurate AGT ranging from the lambda point of helium $T_\lambda = 2.172$ K to the freezing point of copper $T_{Cu} = 1358$ K.

1.1. Absolute primary AGT

Absolute primary AGT exploits the relationship between the speed of sound in a dilute gas u^2 and the thermodynamic temperature T and pressure p of the gas:

$$u^2 = \left(\frac{\partial p}{\partial \rho}\right)_S = \frac{\gamma_0 k_B T}{m} + A_1(T)p + A_2(T)p^2 + \cdots. \quad (1)$$

In equation (1), ρ is the mass density of the gas; S is the entropy; $\gamma_0 \equiv C_p^0/C_v^0$ is the zero-density ratio of the constant-pressure specific heat to the constant-volume specific heat that is exactly 5/3 for the monatomic gases; k_B is the Boltzmann constant and m is the average mass of one atom or molecule in the gas. Exact thermodynamic relationships connect $A_1(T)$ and $A_2(T)$ to the density virial coefficients and their temperature derivatives (Trusler 1991, Gillis and Moldover 1996). For AGT, the speed of sound in monatomic gases has been accurately determined by measuring the acoustic resonance frequencies of gas-filled cavities enclosed by heavy metal walls such as those shown in figure 1.

The first equality in equation (1) was derived from the linearized Navier–Stokes equations which are themselves derived from the Boltzmann equation. Corrections to this equality resulting from the non-zero amplitude of sound (Coppens and Sanders 1968, Hamilton *et al* 2001) and the non-zero frequency of sound (Greenspan 1956) are known; they are negligible at the acoustic amplitudes, gas densities and acoustic frequencies used for AGT. The second equality in equation (1) relies on exact thermodynamic relations between the derivative $(\partial p/\partial \rho)_S$ and the virial coefficients of the equation of state.

Using equation (1), the thermodynamic temperature is deduced from measurements of the speed of sound on an isotherm that are traceable to the metre and the second. For absolute primary AGT using argon, $A_1(T)$ and $A_2(T)$ have always been fitted to measurements of $u(p, T)$ and this is usually done for helium-based AGT. An acceptable alternative to fitting helium isotherms is to rely on the values of $A_1(T)$ and $A_2(T)$ calculated from quantum mechanics and statistical mechanics (Garberoglio *et al* 2011, Cencek *et al* 2012). Gavioso *et al* (2010a) did this when they measured u^2 in helium at 410 kPa to re-determine the product $k_B T_{TPW}$ with a relative standard uncertainty of 7.5×10^{-6}. In their realization of AGT, the uncertainties of $A_1(T)$ and $A_2(T)$ contributed less than 1×10^{-6} to the relative uncertainty of $k_B T_{TPW}$. (Unless otherwise stated, all uncertainties in this work are standard uncertainties with coverage factor $k = 1$ corresponding to a 68% confidence interval.) Because the calculated values of $A_1(T)$ and $A_2(T)$ for helium are functions of the *thermodynamic* temperature, they are part of the model for the realization of AGT.

Since 1979, absolute primary AGT has been conducted only near T_{TPW} and only using highly refined cavity resonators with fixed dimensions to re-determine the product $k_B T_{TPW}$. Several groups have measured the speed of sound in argon or helium near T_{TPW} with relative uncertainties near 1×10^{-6} or less (Moldover *et al* 1988, Gavioso *et al* 2011, Pitre *et al* 2011, de Podesta *et al* 2011, 2013, Zhang *et al* 2011, Lin *et al* 2013). With one exception discussed below, these groups deduced the speed of sound from measurements of the resonance frequencies of the radially symmetric oscillations of helium or argon contained within an approximately spherical cavity using the relation

$$u = \frac{f_a - \Delta f_a}{z_a}(6\pi^2 V)^{1/3}. \quad (2)$$

Here f_a is the measured resonance frequency of the gas oscillation in the mode designated by the subscript 'a', Δf_a is the sum of corrections to the unperturbed resonance frequency $f_{a,0}$, V is the volume of the cavity and z_a is a mode-dependent acoustic eigenvalue that was calculated from the shape of the cavity. (Usually, $f_a < f_{a,0}$ because some of the corrections Δf_a discussed in section 3 are negative.) For the radially symmetric acoustic modes of a nearly spherical cavity, the eigenvalues z_a are not sensitive to smooth, volume-preserving departures from a spherical shape in the first order of perturbation but are sensitive in higher orders of perturbation theory. Thus, z_a can be calculated with a fractional uncertainty on the order of $(5 \times 10^{-4})^2$ for a cavity manufactured to the readily attainable tolerance 5×10^{-4} (Mehl and Moldover 1986). Then, u can be measured with an uncertainty on the

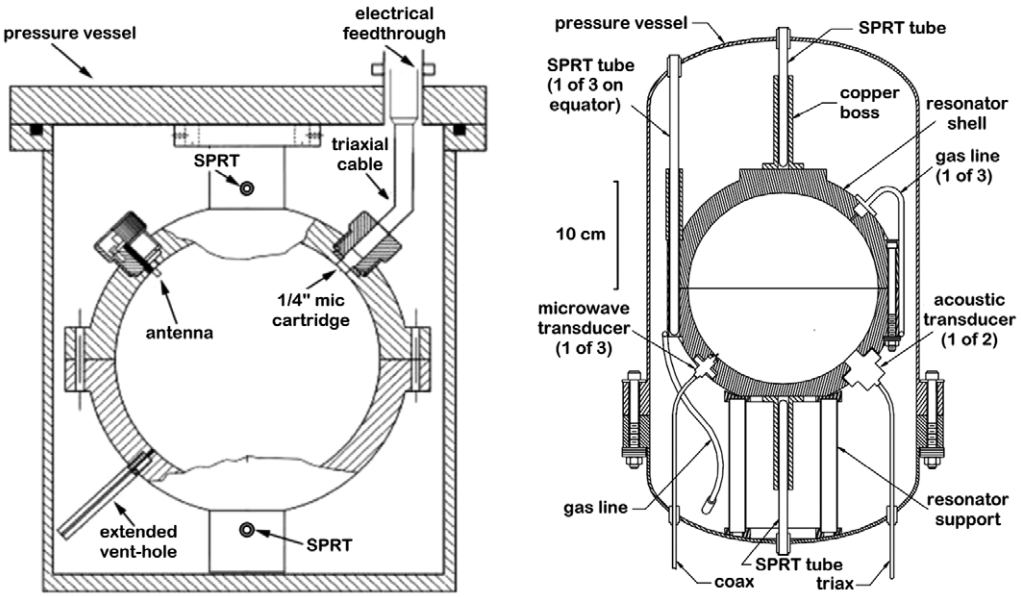

Figure 1. Two acoustic thermometers in their pressure vessels. The thermometer on the left (Benedetto *et al* 2004) had a cavity radius of 60 mm and it was used from 234 K to 380 K. The thermometer on the right (Strouse *et al* 2003) had a cavity radius of 89 mm and it was used from 273 K to 505 K. Later, two acoustic transducers were replaced with ducts and it was used up to 633 K (Ripple *et al* 2013).

order of 10^{-6} if the frequency corrections Δf_a and the cavity's volume V are known with similar uncertainties.

The volume of nearly spherical cavities has been determined with fractional uncertainties of 1×10^{-6} or less by weighing the quantity of mercury (Moldover *et al* 1988) or of water (Underwood *et al* 2012) that just filled the cavity and relying on the literature measurements of the density of these well-characterized liquids. Alternatively, microwave resonances have been used to accurately determine the volume of finely machined, nearly spherical, copper-walled cavities with relative uncertainties on the order of 10^{-6} using the relation

$$c = \frac{n\langle f_m - \Delta f_m\rangle_p}{z_m}(6\pi^2 V)^{1/3} \qquad (3)$$

Here, c is the defined speed of light in vacuum, f_m is the measured microwave frequency, n is the refractive index of the gas in the cavity at the pressure p, z_m is a mode-dependent microwave eigenvalue and $\langle f_m - \Delta f_m\rangle_p$ is the average of the corrected frequencies of the $(2l + 1)$ microwave modes that would be degenerate in a perfect spherical cavity ($l = 1, 2, 3, \ldots$). Usually, only the triply degenerate $l = 1$ modes are used. Equation (3) exploits the theorem that the average frequency of the $(2l + 1)$ modes is invariant in the first order of perturbation theory but sensitive to small, smooth departures from a spherical shape in higher orders (Mehl and Moldover 1986). In one remarkable example, the fractional difference between a microwave volume determination and a weighing volume determination was $(0.46 \pm 1.81) \times 10^{-6}$ (Underwood *et al* 2012).

The microwave measurements are simplified if the cavity has a 'quasi-spherical' shape, that is, a shape that differs from spherical by just enough to separate the degenerate microwave frequencies, but not so much that the accurate calculation of the microwave and acoustic eigenvalues requires detailed measurements of the shape (Mehl *et al* 2004). Typically, a quasi-spherical AGT cavity approximates a triaxial ellipsoid with axes in the ratios $1 : (1 + e) : (1 - e)$ and with $0.0005 < e < 0.001$. For this family of shapes, the electromagnetic eigenvalues z_m are known with extraordinarily small uncertainties (Mehl 2009, Edwards and Underwood 2011). For absolute primary AGT with the lowest possible uncertainties, quasi-hemispherical copper cavities have been manufactured by diamond turning. A pair of carefully aligned, quasi-hemispheres bolted together creates a quasi-spherical cavity. For relative primary AGT, quasi-hemispherical cavities have been machined out of cylindrical billets of stainless steel, aluminium and copper using a numerically controlled milling machine.

The most attractive features of absolute primary AGT conducted with a noble-gas-filled, quasi-spherical cavity resonator are evident when combining equations (1)–(3) to obtain

$$\left[\frac{f_a - \Delta f_a}{z_a}\frac{z_m c}{n\,\langle f_m - \Delta f_m\rangle_p}\right]^2 = \frac{5k_B T}{3m} + A_1(T)p + A_2(T)p^2 + \cdots. \qquad (4)$$

In a first approximation, $k_B T$ is determined by the ratio (speed of sound)/(speed of light) which is proportional to ratios of measured frequencies: $k_B T \approx 3m[f_a z_m c/(z_a n f_m)]^2/5$. The pressure and the dimensions of the cavity only appear in the correction terms such as Δf_a, Δf_m, $A_1(T)p$ and $A_2(T)p^2$.

We emphasize that equation (4) is always applied to measurements made with several different microwave and acoustic modes at each temperature and pressure. This redundancy facilitates very precise tests of the theories for the frequency corrections Δf_a, Δf_m and for the eigenvalues z_a and z_m. Indeed, redundancy distinguishes AGT from other forms of gas thermometry.

Because the leading term of equation (4) contains the ratio T/m where m is average mass of an atom of the gas, the uncertainty of m contributes directly to the uncertainty of T. Commercially prepared helium is predominantly the isotope ^{4}He with a sub-part-per million concentration of the isotope ^{3}He (Mook 2000). Therefore m is well known for ^{4}He that has been chemically purified, for example, by passing through a well-designed liquid-helium cold trap. In contrast, commercially prepared argon has significant concentrations of several isotopes and the isotopic composition changes from bottle to bottle, even from a single supplier. Therefore, it is difficult to determine m of an argon sample with a relative uncertainty on the order of 10^{-6}. However, it has been accomplished using isotopic argon standards and analysis for chemical impurities, including other noble gases (Moldover *et al* 1988, Valkiers *et al* 2010, Mark *et al* 2011, Zhang *et al* 2011).

Quasi-spherical cavities are not essential for accurate, absolute primary AGT. Zhang *et al* (2010, 2011) re-determined $k_B T_{TPW}$ using the non-degenerate, longitudinal acoustic modes of an argon-filled, fixed-path-length cavity. The ends of their cavity were not exactly perpendicular to the cavity's axis; however, this shape imperfection does not change the eigenvalues of the longitudinal modes in the first order of perturbation theory. Thus, a measurement of the average length of the cavity was sufficient for accurate AGT and it was accomplished using two-colour optical interferometry (Zhang *et al* 2011). If all the surfaces of the cavity were conducting, microwave modes could have been used for determining the average length. The non-degenerate radial modes of a cylindrical cavity could also be used for AGT if the average radius of the cylinder were determined from microwave resonances.

For completeness, we note that before 1979, absolute primary AGT was conducted using cylindrical, acoustic cavity resonators containing a movable piston that varied the cavity's length. Measurements in the range from 1.2 K to 423 K achieved standard uncertainties of $10^{-4}\ T$ to $5\times10^{-4}\ T$ (Plumb and Cataland 1966, Grimsrud and Werntz 1967, Gammon 1976). In 1979, Colclough *et al* used a variable-length cavity at T_{TPW} and achieved the low standard uncertainty 8×10^{-6} $k_B T_{TPW}$ (Colclough *et al* 1979). Over the past 30 years, the understanding of cavity resonators, together with their associated transducers and ducts that deliver and remove gas, has increased greatly. In contrast, the mechanical problems of making and using a cylindrical cavity with a movable piston have not changed. Therefore, it is unlikely that variable-length cavities will be used for AGT in the future.

1.2. Relative primary AGT

Relative AGT determines the ratio of two (or more) thermodynamic temperatures from measurements of the ratios of speeds of sound conducted on the isotherms of interest. (We identify one isotherm as the reference temperature T_{ref} and a second isotherm by T.) Relative AGT uses equation (1) at the unknown temperature T and the reference temperature T_{ref} to form the ratio

$$\left[\frac{u(T)}{u(T_{ref})}\right]^2 = \frac{T + m\left[A_1(T)p + A_2(T)p^2 + \cdots\right]/(\gamma_0 k_B)}{T_{ref} + m\left[A_1(T_{ref})p + A_2(T_{ref})p^2 + \cdots\right]/(\gamma_0 k_B)}. \quad (5)$$

In contrast with absolute primary AGT, the ratio $[u(T)/u(T_{ref})]^2$ in equation (5) can be accurately measured without realizing either the metre or the second. The ratio measurement does require measuring ratios of lengths and times (or frequencies) with low uncertainties.

The average mass of an atom m of the thermometric gas does not appear in the leading term in equation (5) because of the implicit assumption that m is identical at T and T_{ref}. Thus, the thermometric gas for relative AGT could be a noble gas composed of several isotopes or a noble gas with a small concentration of noble gas impurities, provided the gas mixture does not fractionate in the acoustic thermometer.

Since 1999, relative AGT has been conducted in the wide temperature range 7 K to 552 K (Moldover *et al* 1999, Ewing and Trusler 2000, Benedetto *et al* 2004, Pitre *et al* 2006, Ripple *et al* 2007). In the sub-range 234 K to 380 K, the results of Benedetto *et al* (2004) overlap the results of either Moldover *et al* (1999) or Ripple *et al* (2007). These independently realized versions of relative AGT had very different experimental details; however, their results agreed within $3\times10^{-6}\ T$. Results from four independent realizations of AGT at the gallium and mercury points agreed within $3\times10^{-6}\ T$ (Pitre *et al* 2006). All these realizations of relative AGT since 1999 used gas-filled, metal-walled, spherical or quasi-spherical cavity resonators to measure speed-of-sound ratios. In these realizations, the microwave and acoustic resonance frequencies of several cavity modes were measured near the temperature of the triple point of water T_{TPW} and the frequencies of the same modes were measured at the other temperatures of interest T. The working equation has the form

$$\left[\frac{(f_a - \Delta f_a)_{T,p}}{(f_a - \Delta f_a)_{TPW,p}}\frac{\langle f_m - \Delta f_m\rangle_{TPW,p}}{\langle f_m - \Delta f_m\rangle_{T,p}}\frac{n(T_{TPW}, p)}{n(T, p)}\right]^2 = \frac{T + \left(\frac{m}{\gamma_0 k_B}\right)\left[A_1(T)p + A_2(T)p^2 + \cdots\right]}{T_{TPW} + \left(\frac{m}{\gamma_0 k_B}\right)\left[A_1(T_{TPW})p + A_2(T_{TPW})p^2 + \cdots\right]}. \quad (6)$$

Equation (6) exploits the fact that the ratios (acoustic frequencies)/(microwave frequencies) depend upon the cavity's volume but not upon details of the cavity's shape. Shape perturbations that might be unacceptably large for absolute primary AGT based on equation (4) may be acceptable for relative primary AGT because the calculated eigenvalues do not appear in equation (6). Indeed, the cavity plays a limited role in measuring u/c.The cavity is a temporary artefact that satisfies three conditions: (1) its dimensions are stable during the measurements of $f_a(p)$ and $\langle f_m(p)\rangle$ at the temperature T, (2) the changes in its eigenvalues between T and T_{TPW} are within the desired tolerance (small, smooth changes in the shape of the cavity, such as those caused by anisotropic thermal expansion (Moldover *et al* 1999, Pitre *et al* 2006) affect the eigenvalues only in the second order and higher

orders) and (3) any difference between the cavity's acoustic and microwave volumes (resulting, for example, from an oxide layer) are nearly constant between T and T_{TPW}.

In practice, equations (4) and (6) are rewritten in the form $0 = F(x_{\mathrm{meas}}, x_{\mathrm{calc}}, x_{\mathrm{fit}})$ where the measured quantities x_{meas} include the frequencies f_{a}, f_{m}, T_{90}, the pressure (or density) and quantities measured in auxiliary experiments such as m and A_3. The calculated quantities x_{calc} include the corrections Δf_{a}, Δf_{m}, and may include thermodynamic quantities such as $(\partial u^2/\partial p)_{\mathrm{T}}$. Finally, ΣF is minimized to determine the fitted quantities x_{fit} including T and apparatus parameters such as A_{-1} and A_1. (As discussed in section 5.2, accounting for the non-zero mean free path of the gas adds terms of the form $A_{-1}(T)p$ to the sums in the square brackets on the right-hand side of equation (6).) The summation ΣF is weighted to account for measurement uncertainties and ΣF always contains data that span a range of pressures and include several microwave and acoustic modes.

Equation (6) may be used with sufficient accuracy within a degree or so of T_{TPW}; it is not necessary to set a gas thermometer to exactly T_{TPW}. We expect that some AGTs will use equation (6) or its equivalent with reference temperatures T_{ref} far from T_{TPW}. For example, one relative primary AGT might be used to accurately measure the thermodynamic temperature of the hydrogen point $T_{\mathrm{H_2}}$ and a second AGT, specifically adapted to low temperature measurements, might be referenced to $T_{\mathrm{H_2}}$.

Many of the specialized, absolute primary AGTs that were developed to re-determine $k_{\mathrm{B}}T_{\mathrm{TPW}}$ used circulating liquid baths for the outermost stage of their thermostats. After comparatively minor modifications of their thermostats, these thermometers could be used for absolute primary AGT throughout a modest range of temperatures, both above and below T_{TPW}. It is unlikely that any of these instruments could function at temperatures well above T_{TPW}, where the reliability of transducers and the stability and mutual compatibility of materials drive the design of all thermometers. Instead, high-temperature acoustic thermometers will use apparatus designed for the environment and will rely on speed-of-sound ratio measurements instead of more difficult absolute measurements (Ripple 2003).

2. Measuring resonance frequencies

2.1. Acoustic and microwave transducers

2.1.1. Acoustic transducers. Accurate AGT requires a sound generator and a sound detector that perturbs the cavity's acoustic and microwave resonances in only small, predictable ways. The transducers should have a smooth frequency response; however, a flat response is not necessary. If the transducers are mounted either in or on the cavity's shell, they must not contaminate the thermometric gas. Ideally, the only coupling between the sound generator and sound detector is through the gas in the cavity. Thus, the transducers should have a small moving mass to minimize their coupling through the shell's recoil. These criteria have been satisfied by home-made electret microphones, small, commercially manufactured, capacitive microphones, piezoelectric (PZT) 'benders' and remote transducers coupled to the cavity by ducts.

If a capacitive microphone is directly exposed to the thermometric gas, it should be assembled from ceramic and metal parts but not from polymers to minimize the chances of contaminating the gas. The moving part of the capacitor is thin (typically, 7×10^{-6} m thick), fragile, stretched, metal, membrane with a very low mass. For generating sound, the capacitor can be driven by an alternating voltage at the frequency f, either with or without a dc bias voltage. With a dc, bias, its diaphragm will oscillate at the frequency f; without a bias, the oscillation will be at frequency $2f$. Operation in the $2f$ mode circumvents electrical cross-talk that might occur between the large driving voltage and the small voltage generated by the detector. Typically, the maximum allowable voltage (dc + alternating) applied to a capacitive microphone is approximately 200 V. Larger voltages may cause an arc that will destroy the diaphragm. The maximum allowable voltage depends upon the gas and, for typical capacitors, has a minimum below atmospheric pressure. For a given maximum voltage, a microphone operating in the $2f$ mode will generate a higher acoustic pressure than one operating in the dc-biased mode.

Capacitive microphones have been mounted with their membranes flush with the inside wall of a cavity where they generate only small perturbations to the microwave resonance frequencies. Because of their small size and small gas-filled volume, the microphones produce only small, predictable (and experimentally verified) perturbations to the acoustic resonance frequencies (Guianvarc'h *et al* 2009). When used as a detector, capacitive microphones require a large dc bias voltage and precautions to minimize the parasitic capacitance between the detector and a high-impedance preamplifier. (Some have used a triaxial cable with a driven guard electrode leading from the detector to a high-impedance, remote preamplifier.) At temperatures above approximately 550 K, Ripple *et al* (2007) observed unacceptably high noise that resulted from erratic electrical leakage through ceramic cable insulators subjected to a high-voltage bias. The electrical dissipation within capacitive microphones is negligible.

In contrast with capacitive microphones, ceramic piezoelectric transducers are rugged, massive, have low electrical impedances, and can generate higher acoustic pressures. Zhang *et al* (2011) mounted lead-zirconate-titanate (PZT) piezoelectric transducers on the outside of cavity resonators and coupled them to the gas inside the cavity through a 0.2 mm to 0.3 mm thick diaphragm machined into the wall of the cavity. Thus, their PZT transducers did not contact the gas inside the cavity and could not contaminate it. The comparatively thick coupling diaphragm changed neither the shape nor the electrical conductivity of the interior surface of the cavity; therefore, it would not perturb the microwave resonance frequencies of the cavity if they had been measured. Piezoelectric transducers generate small predictable perturbations to the acoustic modes of the cavity. Lin *et al* (2010) used a PZT transducer to generate sound; when it was driven with RMS voltages V_{PZT} up to 7 V, it dissipated the power $(P/\mu\mathrm{W}) = 5 \times 10^{-3}(f/\mathrm{kHz})^{1.83}(V_{\mathrm{PZT}}/\mathrm{V})^2$. Zhang

et al did not report problems resulting from mechanical coupling of PZT transducers to the walls of the cavity. One of us (JTZ) recommends using a PZT transducer as a sound generator and a capacitive microphone as a sound detector to increase the signal-to-noise ratio of acoustic measurements while halving the acoustic-transducer-generated perturbations to the acoustic and microwave frequencies.

Ripple *et al* (2013) used a duct to conduct sound from a remote piezoelectric sound generator at ambient temperature into a cavity resonator at 600 K and a second duct to conduct sound out of the cavity to a remote commercially manufactured sound detector at ambient temperature. This arrangement enabled AGT at high temperatures where commercially manufactured capacitive microphones and piezoelectric transducers do not operate. Theory is helpful for guiding the design of such ducts and for computing the small perturbations they generate to the acoustic resonance frequencies of the cavity (Gillis *et al* 2009). As the amplitude of the acoustic flow in a duct is increased, the flow will transition from a laminar profile to a turbulent profile and the dissipation in the duct will increase (Olson and Swift 1996). However, this condition is unlikely to occur during AGT.

Ewing and Trusler (2000) successfully used home-made electret transducers between 300 K and 90 K. Their transducers had thin polymer films in contact with the gas, which may be incompatible with maintaining gas purity at higher temperatures.

At resonance, typical acoustic pressures $\wp$ in the cavity are in the range $0.1\ \text{Pa} < \wp < 1\ \text{Pa}$. Hamilton *et al* (2001) predict that the perturbation of the resonance frequencies by nonlinear effects will be $(\Delta f/f)_{\text{nonlinear}} \approx [(\gamma-1)Ma/8]^2$, where $Ma \equiv |\wp|/(\rho u^2)$ is the acoustic Mach number. This condition sets an upper bound to the sound pressure for accurate AGT. If a duct transmits high-amplitude sound into a cavity, vortices may form at the cavity's entrance. This phenomenon may set another bound on the maximum sound pressure.

2.1.2. Coupling microwaves to the cavity. All the measurements of microwave frequency resonances used in AGT have used one coaxial cable to conduct the microwave fields from the generator (preferably, a network analyser) to the cavity and a second cable to conduct the fields transmitted through the cavity back to the detector (the same vector analyser). Near the inner wall of the cavity, both cables are terminated by antennas. The simplest antenna is a short, straight extension of the inner conductor. The perturbations to the microwave frequencies produced by this kind of antenna have been modelled quantitatively and verified by measurements (Underwood *et al* 2010). However, straight antennas only couple to the TM family of modes. Alternatively the cables can be terminated with a wire loop that connects the centre conductor of the cable to the outer conductor of the cable. Such loops couple to all the modes of the cavity and Pitre *et al* (2006, 2011) measured the frequency perturbations produced by the loops using a substitution method.

The wires or loops used to couple microwaves will perturb the acoustic resonance frequencies. These perturbations have been considerably reduced by recessing the wires or loops in holes in the cavity's wall and then filling the recesses with a material such as epoxy or vacuum grease which is transparent to the microwaves. If the filling material has a high acoustic impedance and terminates at the surface of the cavity, its perturbations to the acoustic frequencies will be negligible. (Caution: outgassing from the filling material may contaminate the thermometric gas in the resonant cavity, leading to other problems. See section 9.) The perturbations from imperfect terminations are discussed in detail by Pitre *et al* (2011) in their section 4.4.2.

Recently, Feng *et al* (2013a) demonstrated that home-made, coaxial cables insulated with fused silica beads are suitable for AGT at temperatures up to 1350 K. The microwave signal-to-noise ratios were satisfactory and pure argon gas could be flowed through the cable to avoid oxidation of the cables' centre and outer conductors. These cables, in conjunction with the acoustic transducers and ducts used by Ripple *et al*, imply that AGT can be effectively conducted up to 1350 K.

2.2. Acquiring and fitting frequency data

For accurate realizations of AGT, we recommend measuring the acoustic resonance frequencies and the microwave resonance frequencies at the same time, that is, while the thermometric gas is in the cavity. When this is done, the volume (and the average radius) of the cavity at the pressure under study is determined from the product $n(f_{\text{m}} - \Delta f_{\text{m}})$ using equation (3) and no correction is needed for the deformation of the cavity under hydrostatic pressure. (See section 8.1 for the values of the refractive index.)

Approximate values of the acoustic resonance frequencies f_{N} and half-widths g_{N} are obtained from either preliminary measurements or a model. Then, the sound generator driven by a frequency synthesizer is stepped through discrete frequencies and the in-phase u and quadrature v signals at the detector are measured using a lock-in amplifier. Before making a voltage measurement at each frequency, it is necessary to wait a multiple of the longest relaxation time needed to reach a steady state. For frequencies near f_{N}, the acoustic pressure in the cavity approaches its steady-state value as $\exp(-\theta/\tau_{\text{a}})$ where θ is the elapsed time and $\tau_{\text{a}} \equiv 1/(2\pi g_{\text{N}})$. Therefore, a wait on the order of $10\tau_{\text{a}}$ is required for the voltage to reach 10^{-4} of its final value. The required wait will be longer than $10\tau_{\text{a}}$ if either the post-detection time constant of the lock-in amplifier or the settling time of the frequency-tracking circuit of the lock-in amplifier is longer than τ_{a}. A simple protocol uses 11 frequencies starting at $f_{\text{N}} - g_{\text{N}}$ and ending at $f_{\text{N}} + g_{\text{N}}$ with steps of $g_{\text{N}}/5$. Then, the frequency sweep is reversed by starting at $f_{\text{N}} + g_{\text{N}}$ and ending at $f_{\text{N}} - g_{\text{N}}$ with steps of $-g_{\text{N}}/5$. Alternative protocols, such as using more frequencies, taking data over a range wider than $f_{\text{N}} \pm g_{\text{N}}$, and spacing the points at selected, unequal frequency intervals, will reduce the uncertainty of the fitted parameters in many circumstances. The frequencies and complex voltages are fitted by the resonance function:

$$u + \mathrm{i}v = \frac{\mathrm{i}fA}{f^2 - (f_{\text{N}} + \mathrm{i}g_{\text{N}})^2} + B + C(f - \tilde{f}) + D(f - \tilde{f})^2, \quad (7)$$

where A, B, C and D are complex constants; $F_N = f_N + ig_N$ is the complex resonance frequency of the mode N under study and the parameter $\tilde{f}$ is fixed at an arbitrary value near f_N. The parameters C and D account for the effects of possible cross-talk and the 'tails' of the modes other than N. At high gas densities, the term $D(f - \tilde{f})^2$ may not be significant. At low densities, corrections to equation (7) may be needed (section 3.1). Because the parameters f_N and g_N appear in the denominator of equation (7), iterative, non-linear fitting routines are used.

For AGT, the microwave resonance frequencies are determined by sweeping through triplets of microwave resonances. Typically, data are acquired at 100 or more frequencies and they are fitted to a generalization of equation (7) that contains a sum of three terms with resonance denominators. Then, the fitting function has three complex values of A, three values of f_N and three values of g_N in addition to the background terms. For an ideal cavity, the three values of g_N would vary as $(f_N)^{-1/2}$; in practice, the values of g_N are larger for the modes that have currents crossing the joint between the quasi-hemispheres than for the modes with currents parallel to the joint. (For particular diamond-turned copper spheres the 'joint' effect on g_N was only $\sim 2 \times 10^{-7} f_N$.) Because the microwave Qs are a factor of 10 or more larger than the acoustic Qs, corrections to the microwave frequencies of order $1/Q^2$ have a negligible effect on k_B.

The frequency references for the microwave vector analyser and the frequency synthesizer that drives the sound generator may be locked together. If this is done, errors that might arise from inaccuracies in either reference frequency cancel out of the ratios f_a/f_m which appear in equations (4) and (6).

3. Theoretical corrections to acoustic resonance frequencies

Here, we discuss corrections to the raw acoustic data that are based on reliable theories. (Benedetto *et al* (2004) published a compact list of the corrections for a spherical cavity; in online supplement A (stacks.iop.org/Met/51/R1/mmedia), we reproduce this list after making minor additions and corrections. Zhang *et al* (2011) published a similar list of the corrections for a cylindrical cavity.) The theory for the half-widths of the acoustic resonances requires accurate values of the viscosity and thermal conductivity of the thermometric gas (section 3.4). However, the theory does not contain parameters that are determined from AGT. Thus, a comparison of the theory of the half-widths obtained with a particular acoustic thermometer provides a parameter-free assessment of the understanding of that thermometer under the conditions of use.

3.1. Thermal and viscous boundary layers

During each acoustic cycle, heat exchange between the gas and the shell surrounding the cavity results in a thermo-acoustic boundary layer in the gas that is characterized by an exponential decay length $\delta_T \equiv [\lambda/(\rho C_p \pi f)]^{1/2}$. Here λ is the thermal conductivity of the gas, ρ is its mass density, C_p/M is the constant-pressure molar heat capacity (which is exactly $5R/2$ for monatomic gases in the limit of zero density) and M is the average molar mass. For the radially symmetric acoustic modes of a spherical or quasi-spherical cavity with radius a, the boundary layer contributions to the real and the imaginary (half-width) parts of the resonance frequencies are

$$\frac{\Delta f_{\rm therm} + i g_{\rm therm}}{f_{a,0}} = \left((-1+i)(\gamma - 1)\frac{\delta_T}{2a} - i(\gamma - 1)(4\gamma - 2)\left(\frac{\delta_T}{2a}\right)^2 \right) \times \left[1 - \frac{(\delta_T \lambda)_{\rm shell}}{(\delta_T \lambda)_{\rm gas}} \right], \quad (8)$$

where $f_{a,0}$ is the unperturbed resonance frequency. Thus, $\Delta f_{\rm therm}$ and $g_{\rm therm}$ are equal and both increase at low density as $\rho^{-1/2}$. For typical AGT, $50 \times 10^{-6} < \Delta f_{\rm therm}/f < 200 \times 10^{-6}$ and this is the largest correction to the raw data. The corresponding fractional corrections to $\Delta T/T$ are $100 \times 10^{-6} < \Delta T/T < 400 \times 10^{-6}$.

The term in square brackets on the right-hand side of equation (8) accounts for the penetration of the thermal oscillations into the shell (Moldover *et al* 1988). This correction will be important when AGT is conducted in copper-walled cavities below 10 K. Measurements at low densities have detected the term proportional to $(\delta_T/2a)^2$ (Gillis 2012). Often, an equation similar to equation (8) is written where $f_{a,0}$ is replaced by f_a, the measured resonance frequency. In that case, the entire term proportional to $(\delta_T/2a)^2$ should be multiplied by $\frac{1}{2}(3\gamma - 1)/(2\gamma - 1) \approx 6/7$.

In equation (8), the term $(-1+i)(\gamma - 1)\delta_T/(2a)$ is both the largest correction to the measured resonance frequencies and the largest contributor to the half-widths of the acoustic resonances. Therefore, the measurements of the half-widths are a critical test of the theory of the boundary layer correction. The agreement between measurement and theory is remarkable. In fact, Gillis (2012) was motived to derive the correction of order $(\delta_T/a)^2$ by the observation that the sum $(g_{\rm therm} + g_{\rm vol})/f$ obtained from equations (8) and (11) was greater than the measured values $g_{\rm meas}/f$ by $\sim 2 \times 10^{-6}$ at low densities.

In a cylindrical cavity, momentum exchange between the oscillating gas and the nearly stationary walls of the cavity results in a viscous boundary layer in the gas that is characterized by an exponential decay length $\delta_v \equiv [\eta/(\rho \pi f)]^{1/2}$, where η is the viscosity. Both the viscous boundary layer and the thermal boundary layer lead to mode-dependent perturbation to the frequencies and half-widths. For the longitudinal modes of a cylinder these are

$$\frac{\Delta f_{\rm therm} + i g_{\rm therm}}{f_{a,0}} + \frac{\Delta f_{\rm visc} + i g_{\rm visc}}{f_{a,0}} = (-1+i)(\gamma - 1)\frac{\delta_T}{2a}\left(1 + \frac{2a}{L}\right) + (-1+i)\frac{\delta_v}{2a}, \quad (9)$$

where a and L are the radius and length of the cylinder, respectively (Zhang *et al* 2011). Because the energy losses from momentum exchange and heat exchange add, the Qs

of the radially symmetric modes of a spherical cavity are approximately five times larger than the Qs of the longitudinal acoustic modes of a cylindrical cavity of length L if both cavities have the same radius a and $L \approx 2a$. For the same reason, the frequency corrections are approximately five times larger ($250 \times 10^{-6} < \Delta f_{\rm therm}/f < 1000 \times 10^{-6}$) at the same pressures. To reduce these corrections, the optimum pressures for AGT conducted with a cylindrical cavity are probably higher than the optimum pressures for AGT conducted with a spherical cavity.

For cylindrical cavities, Lin *et al* (2013) developed an expression (their equation (8)) for $g_{\rm therm} + g_{\rm visc}$ that includes terms proportional to $[\delta_{\rm T}/(2a)]^2$ and $[\delta_{\rm v}/(2a)]^2$ and reduces to equation (9) for small values of these terms. The thermal and viscous boundary layer terms proportional to $[\delta_{\rm T}/(2a)]^2$ and $[\delta_{\rm v}/(2a)]^2$ do not affect the acoustic resonances frequencies of either spherical or cylindrical cavities.

For convenience, we define the surface contribution to the Q of a cavity by $(Q_{\rm surf})^{-1} = 2(g_{\rm therm} + g_{\rm visc})/f$. When raw acoustic data are acquired at low gas densities and fitted by the resonance function, equation (7), the values $f_{\rm fit}$ and $Q_{\rm fit} \equiv f_{\rm fit}/(2g_{\rm fit})$ resulting from the fit should be corrected to account for the frequency dependence of g in the resonance formula. Gillis *et al* (2004) deduced the formulae

$$\frac{f_{\rm corr} - f_{\rm fit}}{f_{\rm fit}} \approx -\frac{1}{8}Q_{\rm surf}^{-2} \quad \text{and} \quad Q_{\rm corr}^{-1} - Q_{\rm fit}^{-1} \approx -\frac{1}{4}Q_{\rm surf}^{-2}. \tag{10}$$

Smaller corrections of order $1/Q^2$ are generated by the second order correction to the thermo-acoustic boundary layer, sound attenuation throughout the volume of the gas $Q_{\rm vol}$ (Gillis *et al* 2004), and by the background terms $C(f - \tilde{f})$ and $D(f - \tilde{f})^2$ in equation (7).

3.2. Attenuation of sound

Under the conditions of AGT, the shift the resonance frequency caused by the attenuation of sound throughout the volume of a resonant cavity is negligible; however, the attenuation adds a term to the half-widths of the acoustic modes given by

$$\frac{g_{\rm vol}}{f_{\rm a}} = \left(\frac{\pi f}{u}\right)^2 \left[\frac{4}{3}\delta_{\rm v}^2 + (\gamma - 1)\,\delta_{\rm T}^2\right]. \tag{11}$$

3.3. Smaller acoustic perturbations

The literature contains calculations of the perturbations to the complex acoustic resonance frequencies resulting from ducts that conduct gas (and sound) into and out of a cavity (Mehl *et al* 2004, Gillis *et al* 2009), holes drilled through the shell (a short duct terminated by a large volume) (Moldover *et al* 1986), acoustic transducers (Guianvarc'h *et al* 2009), and slits that might surround a transducer or a cable (Mehl *et al* 2004). As discussed in section 2.1.2, the acoustic effects of straight and looped microwave antennas at and below ambient temperature have been circumvented rather than modelled. Perhaps this approach can be extended to high temperatures by replacing epoxy with an alternative, high-temperature material. Otherwise, models must be developed for absolute primary AGT. For relative primary AGT, the geometry of ducts, ports, antennas and other shape perturbations should be designed so that the perturbations largely cancel when measuring ratios of thermodynamic temperature. A well-designed AGT will ensure that the difficult-to-measure narrow dimension of any slit is much smaller than $\delta_{\rm v}$ so that the perturbation from the slit is small.

3.4. Thermophysical properties of helium and argon

Accurate values of the density ρ, thermal conductivity λ, and viscosity η of the thermometric gas are required to correct the measured acoustic frequencies for the thermo-viscous boundary layer and sound attenuation. Accurate values of the density are also needed to calculate the refractive index.

The density is calculated from the measured pressure and temperature using the virial equation of state. For helium, remarkably accurate values of the second density and acoustic virial coefficients [$B(T)$ and $\beta_{\rm a}(T) \equiv (M/\gamma_0)(\partial u^2/\partial p)_{\rm T}$] were calculated by Cencek *et al* (2012) and accurate values of the third density and acoustic virial coefficients [$C(T)$ and $\gamma_{\rm a}(T) \equiv (M/2\gamma_0)(\partial^2 u^2/\partial p^2)_{\rm T}$] were calculated by Garberoglio *et al* (2011).

The most accurate, zero-density values of the thermal conductivity and viscosity of helium were calculated *ab initio* from quantum mechanics and statistical mechanics with a fractional uncertainty on the order of 10^{-5} near ambient temperature (Cencek *et al* 2012). Thus, the uncertainty of these transport properties makes a negligible contribution to the uncertainty of helium-based AGT.

For argon, *ab initio* calculations and theory-based correlations are rapidly improving. One of us (Mehl 2013) calculated $B(T)$ and $\beta_{\rm a}(T)$ semi-classically throughout the temperature range $80\,{\rm K} < T < 1500\,{\rm K}$ using the *ab initio* Ar–Ar potential of Patkowski and Szalewicz (2010). The results are tabulated in online supplement B to this paper (stacks.iop.org/Met/51/R1/mmedia). The results for $B(T)$ are consistent with the best available measurements and also with independent calculations of $B(T)$ made by Vogel *et al* (2010) using a different potential. When AGT is conducted using argon-filled resonators with well-understood recoil corrections (section 5.1), the resulting values of $\beta_{\rm a}(T)$ may be more accurate than the *ab initio* values of $\beta_{\rm a}(T)$.

Using a non-additive potential, Jäger *et al* (2011) calculated $C(T)$ for argon and Jäger (2013) calculated higher virial coefficients. At low-to-moderate densities, Jäger's results are consistent with the multi-parameter, empirical equation of state developed by Tegeler *et al* (1999) from fitting measurements. Independently, Cencek *et al* (2013) calculated $C(T)$ and estimated its uncertainty $u(C)$. The results of Cencek *et al* and of Jäger agree: $|C_{\rm Cencek} - C_{\rm Jäger}|/u(C) \leqslant 0.5$ throughout the range $84\,{\rm K} < T < 1500\,{\rm K}$.

One of us (Mehl 2013) calculated $\eta_{\rm Ar}$ and $\lambda_{\rm Ar}$ classically. This calculation also spans the range $80\,{\rm K} < T < 1500\,{\rm K}$ and uses the *ab initio* Ar–Ar potential of Patkowski and Szalewicz (2010). As estimated from the uncertainty of this potential, the relative uncertainties $u_{\rm r}(\eta_{\rm Ar}) \approx u_{\rm r}(\lambda_{\rm Ar}) \approx 0.001$ at 80 K. These uncertainties decrease to $u_{\rm r}(\eta_{\rm Ar}) \approx u_{\rm r}(\lambda_{\rm Ar}) \approx 0.0002$

at 400 K and then increase to $u_r(\eta_{Ar}) \approx u_r(\lambda_{Ar}) \approx 0.0005$ at 1000 K. (See online supplement B for tables (stacks.iop.org/Met/51/R1/mmedia).) Mehl's (2013) results are consistent with the results obtained by Vogel *et al* (2010) from a classical calculation that used an independently derived, *ab inito* Ar–Ar potential; however, Vogel *et al* did not estimate the uncertainties η_{Ar} and λ_{Ar} from their potential. In addition to uncertainties from the Ar–Ar potential, the calculated zero-density values of η_{Ar} and λ_{Ar} have hard-to-quantify uncertainties at low temperatures because they do not account for quantum effects and possible anomalous bound-state effects. Because of these uncertainties in theory, comparisons with measurements in argon are important. We note that May *et al* (2007) searched for anomalous bound-state effects in η_{Xe} and did not find any at the reduced temperature $T/T_{critical} = 0.69$ which corresponds to 104 K in argon.

In the range $200 < T/K < 400$, the accurate values of η_{Ar} can be determined by combining the viscosity of helium η_{He} calculated by Cencek *et al* (2012) with the measurements of the zero-density ratio $\eta_{Ar}/\eta_{He} \equiv$ (viscosity of argon)/(viscosity of helium) by May *et al* (2007) or, very recently, by Zhang *et al* (2013). In this temperature range, Cencek *et al* claim the relative uncertainty $u_r(\eta_{He}) = 0.000\,010$ and May *et al* claim (in their table VI) the relative uncertainties $u_r(\eta_{Ar}/\eta_{He}) = 0.000\,24$ and $u_r(\eta_{Ar}) = 0.000\,84$. The relative uncertainty of $u_r(\eta_{Ar})$ can be reduced from 0.000 84 to 0.000 24 by replacing the values of η_{He} used by May *et al* with the more recent values of η_{He} calculated by Cencek *et al* (2012). In the same temperature range, the thermal conductivity of argon λ_{Ar} can be obtained by combining η_{Ar} with calculated values of the Prandtl number $Pr_{Ar} \equiv (C_p\eta/\lambda)_{Ar}$. Because the Prandtl number depends only weakly on the Ar–Ar interatomic potential, $u_r(\lambda_{Ar}) \approx u_r(\eta_{Ar}) \approx 0.000\,24$. Thus, the uncertainties of η_{Ar} and λ_{Ar} obtained from ratio measurements are comparable to the uncertainty from the *ab intio* calculation, and the measurements and the calculations are mutually consistent in the range $200 < T/K < 400$.

To summarize, η_{Ar} and λ_{Ar} are well known at temperatures above 200 K and they are tabulated in online supplement B (stacks.iop.org/Met/51/R1/mmedia) of this paper. Below 200 K, the uncertainties of η_{Ar} and λ_{Ar} are poorly known; therefore, argon-based AGT below 200 K would benefit from extending the viscosity ratio measurements to lower temperatures.

For completeness, we note that the *ab initio* calculations of $\eta(T)$, $\lambda(T)$, $B(T)$ and $\beta_a(T)$ of helium and argon yield results as a function of the thermodynamic temperature T, not as a function of T_{90}. However, the dependence of AGT on these properties (but not the speed of sound) is sufficiently weak that the differences between T and T_{90} can be ignored in this context.

4. Theoretical corrections to the microwave resonance frequencies

4.1. Microwave boundary layer

The penetration of the microwave fields into the wall bounding the cavity contributes to the half-widths of the microwave resonances g_m and reduces the resonance frequencies by the same amount. For the TM modes in a quasi-spherical cavity these perturbations are

$$\frac{\Delta f_m + i g_m}{f_m} = (-1+i)\frac{\delta_m}{2a}\left(1 - \frac{2}{z_m^2}\right)^{-1}$$
$$\text{with } \delta_m = \frac{1}{\sqrt{\pi f_m \mu \sigma}}. \qquad (12)$$

In equation (12), δ_m is the microwave penetration length, z_m is a microwave eigenvalue, and μ and σ are the magnetic permeability and conductivity of the shell, respectively. (For the TE modes, the term $2/z_m^2$ in equation (12) is absent.) For a non-magnetic stainless-steel wall near ambient temperatures, Moldover *et al* (1999) assumed that $\mu \equiv \mu_0$ (the permeability is identical with the permeability of free space) and $\sigma \equiv \sigma_{f=0}$ (the conductivity is identical to the conductivity of the bulk metal measured near zero frequency). The assumption $\sigma \equiv \sigma_{f=0}$ is usually a good approximation near ambient temperature; however, it fails badly for copper at low temperatures where σ in the thin penetration layer ($\delta_m \sim 1\,\mu$m) is sensitive to impurities and strain that may remain after machining and/or polishing and to the anomalous skin effect (section 4.3). However, the small value of δ_m implies that AGT is relatively insensitive to this assumption (Mehl *et al* 2004). Instead of estimating δ_m from external measurements, one can calculate δ_m from equation (12) and the measured values of the half-widths g_m for those modes where the currents flow parallel to the seam where the quasi-hemispheres meet. This calculation sets a lower bound to δ_m. Measured values of g_N can exceed theoretical values of g_m because of losses associated with currents that cross the joint between the quasi-hemispheres. This extra contribution to g_m was only of order $2 \times 10^{-7} f_m$ in two diamond-turned, copper quasi-spheres, but larger in other cases.

4.2. Antennas and instruments

Underwood *et al* (2010) made a thorough study of the small perturbations to the microwave resonance frequencies resulting from a cylindrical hole in the wall of a cavity, a junction between a coaxial cable and a cavity, and a straight antenna. If the antenna is no longer than the radius of the cable r_c or hole, all of these perturbations are on the order of $(r_c/a)^3$, which can be less than 1×10^{-6}. Furthermore, Underwood *et al* (2010) showed that the perturbation from the energy conducted out of a cavity by coaxial cables is even smaller.

Home-made coaxial cables that are used at high or low temperature may be long and/or lossy and/or have reflecting junctions. Some microwave vector analysers have a method of compensating for the effects of such imperfect cables. To use this feature, the cables leading to the microwave cavity are temporarily disconnected from the cavity and terminated by a well-defined impedance. Then, a reference spectrum is acquired and stored. Compensation for temperature-dependent cable imperfections may not be possible.

The electrical conductivity of the membranes of the acoustic transducers may be lower than the conductivity of the wall bounding the cavity. This will reduce the microwave

frequencies and increase their half-widths by equal amounts. These changes can be measured by exchanging a transducer with a plug made of the same metal as the wall of the cavity.

4.3. Anomalous skin effect

If AGT is conducted at low temperatures in a copper-walled cavity, the anomalous skin effect should be considered (Podobedov 2009). If the copper is pure enough, the microwave penetration depth at a given frequency calculated from equation (12) may become smaller than the mean free path of the conduction electrons. If so, only a small fraction of the conducting electrons spend enough time within the conducting layer to contribute to the conductivity at microwave frequencies. Then, the microwave conductivity is less than that inferred from measurements made at dc or at lower frequencies and the frequency dependence of the penetration depth is anomalous.

5. Phenomenological corrections to acoustic resonance frequencies

The corrections discussed in sections 3 and 4 are based on reliable theories and, except for the electrical conductivity of the cavity's walls, use parameters that are determined with sufficiently low uncertainties from the cited references that do not rely on AGT. We now consider corrections resulting from two phenomena that limit the range of the measurements used for AGT. At high densities, the limiting phenomenon is the elastic response of the resonator's walls to the acoustic oscillations. At low densities, the gas–shell interaction on the scale of the mean free path of the gas is limiting. The theories for these phenomena involve parameters that must be determined for each acoustic thermometer from measurements using that thermometer.

5.1. Elastic recoil of the resonator's walls

Mehl (1985) calculated the effects of shell motion on the gas resonances within spherical shells of arbitrary thickness. Zhang *et al* (2010) calculated similar effects for gas-filled cylindrical shells. The calculations predict the frequencies of the shell resonances from the elastic properties of the shell; however, they neglect imperfections of the joints where metal parts meet. When a gas resonance is not too close to a shell resonance, the theory predicts that the frequency of the gas resonance is shifted by

$$\frac{(\Delta f_l)_{\mathrm{shell},i}}{f_l} \approx -(\rho u^2)_{\mathrm{gas}} \frac{G_{i,l}}{1-(f_l/f_{\mathrm{shell},i})^2}, \qquad (13)$$

where the subscript l represents the indices of a gas mode, the subscript i represents the indices of a shell mode, and $G_{i,l}$ is a compliance that depends upon the geometry of the shell, the gas mode l, and elastic properties of the resonator's walls. The perturbation $(\Delta f_l)_{\mathrm{shell},i}$ is very nearly a linear function of the pressure on an isotherm because $(\rho u^2)_{\mathrm{gas}}$ is nearly proportional to the pressure under conditions of AGT. Thus, a poor estimate of the compliance $G_{i,l}$ will result in values of the acoustic slopes $A_1(T)$ that differ from mode to mode and are inconsistent with the thermodynamic values of $A_1(T)$ given by $A_1 = u_0^2\beta_a/(RT)$.

The radially symmetric modes of a gas within a perfect, isotropic, spherical shell will be perturbed only by the isotropic 'breathing' mode of the shell. For this case, $G_{0\mathrm{n,breathing}} = \chi_{\mathrm{s,int}} \equiv (1/a)(\mathrm{d}a/\mathrm{d}p_{\mathrm{int}})$ which is the shell's compliance to internal pressure p_{int}. This isolated 'breathing-mode' approximation accurately represented the behaviour of the shell used by Moldover *et al* (1999) for acoustic thermometry from 217 K to 303 K. Their claim of accuracy was supported by: (1) the measured value $f_{\mathrm{breathing}} = 13.2\,\mathrm{kHz}$ is only 3% below the calculated value $f_{\mathrm{breathing}} = 13.6\,\mathrm{kHz}$, (2) the agreement of the calculated acoustic slopes $A_1(T)$ with the values measured with five radial modes (after applying equation (4)) over a range of temperatures, and (3) the agreement of the calculated value of the static compliance $\chi_{\mathrm{s,int}}$ with two independent measurements of $\chi_{\mathrm{s,int}}$. The isolated, breathing-mode approximation worked nearly as well for the much more compliant aluminium resonator studied by Moldover *et al* (1986).

Gavioso *et al* (2010b) measured the frequency perturbations $(\Delta f_l)_{\mathrm{shell},i}$ caused by the recoil of the steel shell of a spherical cavity and of the copper shell of a quasi-spherical cavity. For the steel resonator, $(\Delta f_l)_{\mathrm{shell},i}$ had at least four wide peaks in the range 75% to 100% of the predicted $f_{\mathrm{breathing}}$. For the copper resonator, $(\Delta f_l)_{\mathrm{shell},i}$ had three narrow peaks centred at 85% of the predicted $f_{\mathrm{breathing}}$. Thus, the isolated breathing-mode approximation was a poor description of these two resonators. Finite element models of shells show that small departures from perfect radial symmetry (such as flanges at the equatorial joint between hemispheres or small bosses at the closed end of each hemisphere) lead to only small changes in $f_{\mathrm{breathing}}$ and only weak couplings between the radially symmetric acoustic modes and non-radial modes of the shell.

The three shells mentioned above were assembled by bolting hemispheres together. The breathing-mode model worked well for the only one of the three that had a thin, highly compressed layer of wax sealing the hemispheres together (Moldover *et al* 1999). Perhaps the poor agreement between the model and the data for the other shells resulted from the model's neglect of the joint where the hemispheres meet. For all three shells, the measured half-widths of the radial modes exceed the calculated half-widths by a constant times the pressure: $\Delta g_{\mathrm{N}} = g_{\mathrm{N,meas}} - g_{\mathrm{N,calc}} = A_{\mathrm{N}}p$. There are no accurate predictions for A_{N}. However, Δg_{N} does approach zero with decreasing pressure; therefore, the elastic recoil contributions to A_{N} are unlikely to cause errors in AGT.

Zhang *et al* (2010, 2011) modelled several elastic modes of an ideal cylindrical shell that could be excited by longitudinal gas modes. These included longitudinal stretching, bending of the endplates and centre-of-mass motion. (They also modelled radial stretching.) Using several longitudinal modes, Zhang *et al* (2010, 2011) and Lin *et al* (2013) measured values of $A_1(T_{\mathrm{TPW}})$ that were within 10% of the thermodynamic value of $A_1(T)$, after correcting for the calculated elastic recoil. However, the various values of $A_1(T)$ were not mutually consistent within their type A uncertainties. Perhaps these

inconsistencies could be reduced by improving the elastic models for cylindrical shells.

In summary, the elastic recoil of a cavity's shell cannot be predicted reliably from first principles, although a simple model has worked well in one case. In all cases, the inconsistencies among the acoustic modes approach zero linearly with decreasing pressure. These inconsistencies are a measure of the uncertainty of the temperature arising from the elastic recoil of the cavity's walls. An independent measure of the uncertainty of the temperature is the spread among the values of Δg_N at low gas densities, although this spread can arise from phenomena other than the recoil of the cavity's walls.

Acoustic thermometers operating at high temperatures will encounter larger values of the perturbations $(\Delta f_l)_{\text{shell},i}$ because they will operate at higher pressures (section 6). Thus, they should be designed to reduce the compliances $G_{i,l}$ by making the cavity's walls of a stiff material and as thick as practical and making the joints as stiff as possible. Several spherical acoustic thermometers have operated with the ratio (cavity radius)/(wall thickness) ≈ 5. If the ratio had been 2.5, the elastic corrections would have been half as large.

When a gas mode and a shell mode have nearly identical frequencies, they couple strongly and the frequencies are very sensitive to the shell's properties. The frequencies exhibit an 'avoided crossing' and equation (4) is no longer applicable. Acoustic thermometry should not be conducted in this regime. Near-crossings can be identified by analysing the data from multiple acoustic modes at the same temperature and pressure.

5.2. Effects of non-zero mean free path

Ewing *et al* (1986) discussed the acoustic consequences of the kinetic theory prediction that a temperature jump occurs at a gas–solid interface when heat is transferred across the interface. They concluded that the temperature jump increases the resonance frequencies and leaves the half-widths unchanged. For a monatomic gas, the frequency increase is

$$\frac{\Delta f_l}{f_l} = \frac{(\gamma - 1) l_a}{a} \equiv \frac{A_{-1} p^{-1}}{2u_0^2}$$

$$\text{with } l_a = \left(\frac{\lambda}{p}\right)\sqrt{\frac{\pi m T}{2k_B}}\,\frac{(2-h)}{2h}, \qquad (14)$$

where l_a is the thermal accommodation length. In equation (14), λ is the thermal conductivity, m is the mass of an atom, and h is the thermal accommodation coefficient. (If $h = 1$, l_a equals 1.8 times the mean free path. For argon at T_{TPW}, 100 kPa, and $h = 1$, $l_a = 118$ nm.) The coefficient h accounts for the fraction of the gas molecules incident on the solid that are reflected or re-emitted from the solid with the kinetic energy expected from the solid's temperature. Thus h might depend upon the gas, the temperature and the microscopic conditions of the surface (such as oxidation or the presence of an oil film). The temperature jump adds the term $A_{-1} p^{-1}$ to the polynomial expansion equation (1). Ewing *et al* included this term in a fit to their measurements using an argon-filled, aluminium-walled cavity and found $h = 0.84 \pm 0.05$. For an argon-filled, steel-walled cavity, Moldover *et al* (1988) found $h = 0.93 \pm 0.07$ at T_{TPW}. Ripple *et al* (2007) found the average value $h = 1.02 \pm 0.15$ over the temperature range $271 < T/\text{K} < 552$, with no obvious temperature dependence. Benedetto *et al* (2004) and Pitre *et al* (2006) assumed that $h = 1$ over wide temperature ranges. Gavioso *et al* (2011) determined $h = 0.378 \pm 0.010$ for the thermal accommodation coefficient of helium on a diamond-turned copper-walled cavity. Using this experience as a guide, Moldover (2009) assumed that the uncertainty of h was 0.05 and used this value to estimate a value of the gas density below which acoustic measurements would not reduce the uncertainty of the thermodynamic temperature at T_{TPW} (see section 6). In contrast with these observations, Song and Yovanovich (1987) reported values of h ranging from 0.4 to 0.1 for helium interacting with 'engineering surfaces' over the temperature range 273 K to 1250 K.

Feng *et al* (2013b) studied mean-free path effects for the longitudinal acoustic modes of an argon-filled cylindrical cavity. The velocity of a gas oscillating in these modes is transverse to the solid wall bounding the cavity. In this situation, the same kinetic theory considerations which predict a temperature jump at the gas–solid interface also predict a momentum jump (Trusler 1991). The momentum jump increases the resonance frequencies as p^{-1} and leaves the half-widths unchanged. During the calibration of many spinning-rotor vacuum gauges, accurate values of the momentum accommodation coefficient are determined. Often, the resulting accommodation coefficients were within a few per cent of 1 (Chang and Abbott 2007).

6. Optimizing the range of data acquisition

For a given cavity resonator, there is a range of molar gas densities ρ/M that is most useful for conducting low-uncertainty AGT. (M is the average molar mass of the gas.) Moldover (2009) estimated this range for a quasi-spherical, steel-walled cavity with an inside radius of 5 cm and an outside radius of 8 cm. When filled with argon, the optimum range is $40\,\text{mol}\,\text{m}^{-3} < \rho/M < 200\,\text{mol}\,\text{m}^{-3}$ (corresponding to the pressure range $100 < p/\text{kPa} < 500$ at T_{TPW}). When filled with helium, the optimum range is $130\,\text{mol}\,\text{m}^{-3} < \rho/M < 400\,\text{mol}\,\text{m}^{-3}$ (corresponding to the pressure range $300 < p/\text{kPa} < 900$ at T_{TPW}). Although these estimates are very approximate, we will use them to discuss aspects of AGT.

Below the optimum density, the Qs of the acoustic modes decrease approximately as $p^{-1/2}$ and the signal-to-noise ratio of the frequency measurements decreases as p^{-2}, assuming the sound generator produces an acoustic pressure that is proportional to the static pressure. Also, as the density decreases, the mean free path grows as ρ^{-1}. Therefore, as the density is lowered, the uncertainty of the measured acoustic frequencies grows rapidly and the measured frequencies become increasingly sensitive to the parameter A_{-1} (section 5.2). As the density is increased above the optimum range, the measured acoustic resonance frequencies become increasingly sensitive to the recoil of the cavity's wall (section 5.1) and to the pressure-coefficients $A_3(T)$ and $A_4(T)$ that must be added to equations (1) and (2). Thus, at higher than optimum density, one learns more about the complicated

vibrations of the walls and supports of the cavity and more about the higher virial coefficients of the gas; however, this information has only a small effect on the uncertainty of the thermodynamic temperature.

The lower bound to the optimum density is, like the mean free path, approximately independent of the temperature, provided that the sensitivity of the detector of the acoustic pressure (at the wall of the cavity resonator) can be increased as T^{-1}. The upper density bound decreases with temperature because the magnitude of $A_3(T)$, $A_4(T)$, etc increase at low temperatures.

At temperatures above approximately 90 K, both helium and argon can be used for AGT. When compared at the same temperature and pressure, argon has three advantages: (1) the corrections from $A_{-1}(T)$ are larger in helium than argon because the mean free path in helium is 1.5 times longer than in argon, (2) the Qs of the acoustic resonances are 1.7 times larger in argon than in helium, leading to better signal-to-noise ratios, and (3), the speed of sound in argon is less sensitive to common impurities (section 9). However, acoustic measurements made near the liquid–vapour coexistence curve of argon may be subject to bias from pre-condensation (Mehl and Moldover 1982).

For argon in the range of optimum densities mentioned above, δ_T increases only 19% as the temperature is increased from 273 K to 1200 K and the Prandtl number changes less than 1%. Thus, it is possible to conduct AGT in a temperature-independent range of δ_T and δ_v simultaneously instead of a temperature-independent range of molar densities. (A temperature-independent range of δ_T and δ_v is approximately equivalent to a temperature-independent range of Q.) This alternative is advantageous because difficult-to-model acoustic perturbations that depend upon δ_T and δ_v cancel out of the ratio equation (6). For example, a microwave coupling loop that extends from the end of a coaxial cable into (or nearly into) a cavity resonator will generate acoustic perturbations that are difficult to model because they depend upon the ratios of δ_t and δ_v to many lengths. A high-temperature coaxial cable will generate difficult-to-model perturbations if insulation between the centre conductor and the sheath is not sealed at the cavity's wall. This would occur if, for example, the insulator were quartz tubes or sapphire beads. To the extent that differential thermal expansion can be ignored, such complex perturbations will be temperature independent for measurements conducted at constant values of δ_t and δ_v.

7. Uncertainties from pressure measurements

In the AGT working equations ((3) and (6)), the pressure is used in four ways: (1) explicitly in calculating or fitting the terms $A_1 p + A_2 p^2$ that represent the pressure-dependence of u^2, (2) implicitly, when calculating the density-dependent corrections to the acoustic frequencies such as Δf_{therm}, (3) implicitly, when calculating the refractive index n, and implicitly when fitting the thermal accommodation coefficient h in equation (14). Here, we consider how accurately the pressure must be measured so that each of these uses contributes no more than 10^{-6} to the fractional uncertainty of T.

If $T > 8$ K, u^2 in helium varies by less than 1% in the density range recommended in section 6 ($130\,\text{mol m}^{-3} < \rho/M < 400\,\text{mol m}^{-3}$). If $T > 170$ K, u^2 in argon varies by less than 1% in the density range recommend in section 6 ($40\,\text{mol m}^{-3} < \rho/M < 200\,\text{mol m}^{-3}$). For these 'high' temperatures, a relative pressure uncertainty of 10^{-4} at p_{max} is adequate for determining $u^2(p, T)$, and therefore T with a relative uncertainty on the order of 10^{-6}. (Here p_{max} is the maximum pressure on the isotherm of interest.) If a relative pressure uncertainty of $2 \times 10^{-5} p_{\text{max}}$ is achieved, the low-temperature bounds become $T > 3$ K in helium and $T > 91$ K in argon. If A_1 and A_2 are fitted on each isotherm and their values are not checked against theoretical values, the required pressure uncertainty can be reduced to a requirement for pressure linearity and an accurate pressure zero.

As the pressure is reduced towards the minimum pressure on each isotherm p_{min}, the fractional correction to the thermodynamic temperature from the thermo-acoustic boundary layer $(2\Delta f_{\text{therm}})/f_a$ increases as $p^{-1/2}$ and reaches, approximately, 4×10^{-4} at p_{min} for the (0,2) radial acoustic mode. If the fractional uncertainty of p_{min} is 2.5×10^{-3}, its contribution to the fractional uncertainty of T will be 1×10^{-6}.

Assuming that $b_\mu \equiv 0$, the refractive index is calculated from the density using the Lorentz–Lorenz relation

$$\frac{n^2-1}{n^2+2}\frac{1}{\rho} = (A_\varepsilon + A_\mu) + A_\varepsilon(A_\mu + b_\varepsilon)\rho + A_\varepsilon(c_\varepsilon - 2A_\mu^2 - 2A_\varepsilon A_\mu + A_\mu b_\varepsilon)\rho^2 + \cdots. \quad (15)$$

The density is usually calculated from the measured temperature and pressure and an equation of state from the literature. At the maximum densities mentioned in section 6 ($400\,\text{mol m}^{-3}$ for helium and $200\,\text{mol m}^{-3}$ for argon), $n^2_{\text{argon}} = 1.0025$ and $n^2_{\text{helium}} = 1.000\,62$. If these values of n^2 are measured with an uncertainty of approximately 10^{-6}, they will contribute a fractional uncertainty of approximately 10^{-6} to the fractional uncertainty of T. The pressure is nearly proportional to n^2-1; therefore, the required pressure uncertainties are, fractionally, 1.6×10^{-3} for helium and 4×10^{-4} for argon. At the densities used for AGT, the uncertainty of T from the uncertainty of the equation of state is negligible, except for argon at low temperatures.

On each isotherm, the thermal accommodation coefficient h, or equivalently, the thermal accommodation length l_a must be fitted, together with T, A_1 and A_2. We estimate the mean-free-path correction to the acoustic frequencies $\Delta f_l/f_l = (\gamma - 1)l_a/a$ by assuming $h = 1$ and $a = 50$ mm. As the argon pressure is decreased in the range recommended in section 6, this estimate increases as p^{-1} from 0.5×10^{-6} to 2.4×10^{-6} and the corresponding correction to T increases, fractionally, from 1×10^{-6} to 4.8×10^{-6}. This p^{-1} term is easily distinguished from the $p^0 \propto T$ term, provided that the pressure measurements are a linear function of the true pressure and the zero of the pressure transducer is accurate to within a few per cent of p_{min}.

The pressure uncertainties required for all four uses of the pressure are easily attained except when conducting AGT

Table 1. Constants for estimating the refractive index from the density.

Property	Value/($cm^3\ mol^{-1}$)	Reference
	Helium	
A_ε	0.517 254 19(10)	[a]
A_μ	−0.000 007 921(04)	[b]
$b_\varepsilon(T_{TPW})$	−0.0978	[c]
	Argon	
A_ε	4.142 03(15)	[d]
A_μ	−0.000 0809(6)	[e]
$b_\varepsilon(T_{TPW})$	0.28 to 0.31[f]	[d]
b_ε	0.343	[c]

[a] Lach *et al* (2004).
[b] Bruch and Weinhold (2000). The best theoretical estimate is the Pekeris value in the first row of table 1 of this reference plus the relativistic effect which is row 3 minus row 2.
[c] Rizzo *et al* (2002).
[d] Schmidt and Moldover (2003).
[e] Barter *et al* (1960); average of three literature measurements.
[f] See text.

in helium at very low temperatures (and correspondingly low pressures) where the uncertainty of the thermo-molecular pressure gradient contributes to the pressure uncertainty.

As discussed in section 9, it may be advantageous to conduct AGT while gas flows continuously from a manifold through narrow ducts to and from the cavity. If this is done, a separate duct leading from the cavity to the pressure-measurement system is desirable to make accurate pressure measurements without accounting for flow-generated pressure drops.

8. The refractive index and the density

In section 8.1, we recommend refractive index data for determining the radius of a gas-filled cavity from microwave frequency measurements. In section 8.2, we suggest that replacing the pressure in equations (4) and (6) with the density, as determined from microwave frequency measurements, might be useful for low-temperature AGT.

8.1. Data for the refractive index

For helium, the leading terms A_ε and A_μ in equation (15) are independent of the temperature and are accurately known from theory (see table 1). Using a fully quantum statistical approach, Rizzo *et al* (2002) calculated $B_\varepsilon(T) \equiv A_\varepsilon b_\varepsilon(T)$. Their tabulated values of $B_\varepsilon(T)$ vary from $-0.0016\ cm^6\ mol^{-2}$ at 3.799 K to $-0.0651\ cm^6\ mol^{-2}$ at 407.6 K. (See Cencek *et al* (2011) for classical values of $b_\varepsilon(T)$ and their uncertainty between 77 K and 322 K.)

For argon, the values of A_ε and b_ε in table 1 were determined by Schmidt and Moldover (2003) from measurements of $\varepsilon(p)$ near T_{TPW} and 29 °C. They converted $\varepsilon(p, T)$ to $\varepsilon(\rho, T)$ using the empirical equation of state of Tegeler *et al* (1999) and they noted that the uncertainty of the equation of state of argon dominated the uncertainty of their value of b_ε. Our reanalysis of the same data using the density virial coefficients from Jäger *et al* (2011) yields $A_\varepsilon = 4.141\,83\ cm^3\ mol^{-1}$, which agrees with the originally published value (within combined uncertainties), and $b_\varepsilon = 0.31\ cm^3\ mol^{-1}$. For argon, Rizzo *et al* (2002) calculated $b_\varepsilon(T)$ quantum-mechanically and found that $b_\varepsilon(T)$ decreases from $0.52\ cm^3\ mol^{-1}$ at 100 K to $0.31\ cm^3\ mol^{-1}$ at 408 K.

8.2. Relating the microwave frequencies to the density

The measured frequencies of a microwave multiplet are related to the refractive index by

$$n^2 = \left[\frac{\langle f_m - \Delta f_m\rangle_{vac}}{\langle f_m - \Delta f_m\rangle_p}\right]^2 \left(1 + \frac{p}{3B_T}\right)^2 \approx \left[\frac{\langle f_m - \Delta f_m\rangle_{vac}}{\langle f_m - \Delta f_m\rangle_p}\right]^2 \left(1 + \frac{\rho RT}{3B_T}\right)^2 \approx 1 + 3A_\varepsilon\rho. \quad (16)$$

In equation (16), R is the universal gas constant and the subscripts 'p' and 'vac' denote measurements made at the pressure p and under vacuum, respectively. In equation (16), $B_T \equiv -V/(\partial p/\partial V)_T$ is the isothermal bulk modulus of the *cavity* and it accounts for the shrinkage of the cavity's volume under the hydrostatic pressure of the gas. A typical value for copper and for some steels is $B_T \approx 1.4 \times 10^{11}$ Pa near T_{TPW}. Because the volume of a cavity is defined by several, possibly anisotropic, metal parts fastened together, the effective value of B_T of a cavity may differ from a literature value of B_T for the shell's metal.

In equation (16), the second approximate equality is obtained from equation (15) by making the approximations $n^2 + 2 \approx 3$, $A_m \approx 0$ and $b_\varepsilon \approx 0$. This equality shows that the gas density is determined by A_ε and the ratio of measured frequencies, corrected by the fraction $F \equiv 2RT/(9A_\varepsilon B_T)$. We estimate $F_{He} \approx 0.007$ and $F_{Ar} \approx 0.000\,87$ near T_{TPW}. To deduce the density of helium with a fractional uncertainty of 10^{-4} near T_{TPW}, the relative uncertainty of F_{He} must be less than $10^{-4}/F_{He} \approx 0.014$. It might be difficult to know B_T with this low uncertainty for a cavity assembled out of copper parts. At a lower temperature, for example, 30 K, the required relative uncertainty of F_{He} (and B_T) is 0.17, an easily attained value. Thus, it is feasible to conduct helium-based AGT below 30 K by replacing the pressure in equations (3) and (6) with the density deduced from equations (15) and (16). Because $F_{Ar} = 8.007 \times F_{He}$, argon-based AGT using the density is feasible at and below ambient temperature.

At most temperatures, the values of the second and third dielectric virial coefficients of helium and argon are less than 1/10th of the values of the corresponding density virial coefficients. When fitting a function of the density to such isotherms, $\langle f_m - \Delta f_m\rangle^{-2}(T, \rho)$ will require fewer terms than $p(T, \rho)$.

Equation (16) requires an accurate value of $\langle f_m - \Delta f_m\rangle_{vac}$ at each temperature. Measuring $\langle f_m - \Delta f_m\rangle_{vac}$ may be time consuming because evacuating a cavity through a small duct is slow.

9. Chemical impurities and gas handling

A careful accounting for impurities in the thermometric gas is essential for accurate AGT. The normalized derivative

Table 2. Sensitivity of u^2 to impurities (Moldover *et al* 1988).

Impurity	M/ (g mol^{-1})	γ_0	D^a in He	D^a in Ar
H_2	2	1.4[a]	0.23	0.68
He	4	5/3		0.9
H_2O	18	1.32[a]	−3.93	0.12
Ne	20	5/3	−4.0	0.5
N_2	28	1.4[a]	−6.27	0.03
O_2	32	1.4[a]	−7.3	−0.07
Ar	40	5/3	−9.0	
CO_2	44	1.4[a]	−10.3	−0.37
Kr	84	5/3	−20.0	−1.1
Xe	131	5/3	−31.8	−2.3

[a] Values at 273 K. For polyatomic gases, D and γ_0 are temperature-dependent.

$D \equiv (1/u^2)(\mathrm{d}u^2/\mathrm{d}x)$ of the square of the speed of sound u^2 with respect to the mole fraction x of an impurity measures the influence of impurities on AGT. See table 2.

Except for hydrogen, $|D|$ is at least 8 times larger for helium than for argon. Argon's reduced sensitivity to impurities is one reason that argon is preferred to helium for AGT near ambient temperature. For argon, the values of D are of order 1; therefore, the mole fractions of common impurities must be near or below 10^{-6} to realize absolute AGT with uncertainties on the order of 10^{-6}. For relative AGT, any changes in the mole fractions of common impurities between T and T_{ref} must be consistent with the desired uncertainty. At high temperatures, hydrogen from outgassing is the most common impurity and must receive special attention. (See below.)

Highly purified, commercially supplied gas is the starting point for conducting accurate, relative AGT. The manifold that transports the gas from the supplier's cylinder to the cavity and regulates the gas's flow and pressure should be constructed using high vacuum techniques. These include using tubing and fittings with electro-polished interiors and all-metal, bakeable components (including meters and regulators). Virtual leaks must be minimized and joints should be welded or compression-sealed with metal gaskets. The manifold should include a heated, reactive metal (getter) to remove chemically reactive impurities from the supplier's gas. These precautions should reduce the problem caused by outgassing of water from the ambient-temperature parts of the manifold noted by de Podesta *et al* (2011).

When a well-designed manifold supplies pure gas to an acoustic thermometer, the outgassing of the thermometer itself can contaminate the gas. Ripple *et al* (2003) reported outgassing of hydrogen, probably from the stainless steel shell itself. They used a residual gas analyser to quantify the rate of hydrogen outgassing and reduced the outgassing by baking the apparatus for weeks. Such contamination can be detected and accounted for by monitoring an acoustic resonance frequency while the thermometric gas continuously flows through the cavity. If the outgassing rate is independent of the presence of the flowing gas, there will be a range of flows such that the acoustic resonance frequencies are linear functions of the flow rate with a coefficient that varies inversely as the pressure. In this situation, the measured frequency can be extrapolated to zero flow. Alternatively, one can stop the flow and determine the outgassing rate from measurements of $\mathrm{d}f/\mathrm{d}\theta$, the rate at which the frequency changes. (Here, θ is the elapsed time.) Then, all the measurements can be corrected using that outgassing rate.

Several phenomena should be considered when designing a flow system. Purge paths should be designed so that any outgassing sources (e.g., commercial transducers, mass flow controllers) are downstream of the cavity. Heat exchange between the incoming gas and the thermostat must be sufficient to prevent flow-induced thermal gradients forming in the cavity's walls. Except at very low flow rates, gas entering the cavity from a duct will flow in a jet across the cavity, 'splash' off the wall opposite the entrance, and then mix with the gas already in the cavity (Pitre *et al* 2011). To achieve good mixing in the cavity, the outlet duct should not be opposite the entrance duct.

The jet entering the cavity will dissipate its kinetic energy as it mixes with the gas already in the cavity. If the diameter of the inlet duct is too small, the kinetic energy in the jet may be large enough to generate temperature gradients within the gas inside the cavity. This phenomenon may have been observed by Pitre *et al* (2011). Flow-generated fluctuations of the pressure in the cavity will generate corresponding temperature fluctuations in the gas on time scales of milliseconds to many seconds. Such temperature fluctuations will modulate the acoustic resonance frequencies and can easily be mistaken for excess electronic noise during frequency measurements. To reduce this phenomenon, Ripple *et al* (2003) devised a simple, non-contaminating, rapidly responding flow regulator.

During AGT, noble gas impurities in helium or argon are unlikely to be detected by flow-dependent frequency shifts. For example, a duct transporting helium from ambient temperature to a cold cavity can act as a cold trap that collects the argon impurity over a wide range of flow rates. Then, the composition of the helium in the cavity would be independent of flow, but dependent on the duct's and cavity's temperature, causing an error in the AGT that depended on the mole fractions of the impurities. The error could be detected by comparing the speed of sound in the helium before and after it passed through the cryostat. Argon and neon in the supplied helium gas can be detected using sensitive gas chromatography to compare the sample gas with gravimetrically prepared standards. A liquid-helium-cooled trap will remove argon impurities from helium.

Near ambient temperature, the dielectric polarizability of water vapour is an order of magnitude larger than that of other likely impurities; therefore, simultaneous microwave and acoustic measurements may be helpful in distinguishing the outgassing of water vapour from the outgassing of other impurities.

10. Linking the thermodynamic temperature to T_{90}

The acoustic thermometers described above cannot be inserted into fixed point cells, cryostats, or ovens to measure the temperature of these isothermal environments. Instead, all

AGTs must be designed to facilitate linking the average thermodynamic temperature of the gas in the AGT's cavity to the ITS-90. At near ambient and at cryogenic temperatures, the linkage has been made by installing several capsule-type rhodium–iron thermometers or capsule-type standard platinum resistance thermometers (SPRTs) in the shell surrounding the cavity. At higher temperatures, frequently calibrated, long-stemmed SPRTs must be used to realize the ITS-90 with small uncertainties. Therefore, high-temperature acoustic thermometers should contain thermally anchored thermometer wells to facilitate satisfactory immersion of long-stemmed thermometers and their frequent removal for recalibration (Ripple *et al* 2003).

If the temperature of the shell surrounding the cavity is not uniform, the average gas temperature may differ from the temperature(s) indicated by the SPRTs. The use of multiple SPRTs may detect temperature non-uniformities such as a vertical gradient resulting from imperfections of the thermostat. To estimate the effect of a temperature drift rate $(\mathrm{d}T/\mathrm{d}\theta)$, it is convenient to define two time constants: (1) τ_{shell} which is the relaxation time for decay of thermal gradients in the shell and (2) τ_{gas} which is the relaxation time for gas injected into cavity to come to equilibrium with the shell. The temperature drift generates a temperature gradient in the shell on the order of $(\mathrm{d}T/\mathrm{d}\theta)\tau_{\mathrm{shell}}$ and a temperature gradient in the gas on order of $(\mathrm{d}T/\mathrm{d}\theta)\tau_{\mathrm{gas}}$. If a gas flows into the cavity with the volume rate V' and with the temperature difference ΔT from the cavity's temperature, the flow may generate a temperature non-uniformity as large as $\Delta T V' \tau_{\mathrm{gas}}/V$, where V is the volume of the cavity.

11. Uncertainties of AGT

Acoustic thermometers provide redundant data that are used to test the raw data and the corrections that are applied to the raw acoustic data. Routinely, the resonance frequencies and the resonance half-widths of several acoustic and several microwave modes are measured at each temperature and pressure. The frequencies of the several modes are tested for mutual consistency and the values of the half-widths are tested by comparisons with theory. This redundancy can detect many type B uncertainties.

Up to this point, we discussed single isotherms and pairs of isotherms. In fact, the parameters that are fitted on each isotherm (usually A_1, A_2, A_{-1} and T) discussed in section 1 and section 5.2 account for physical phenomena that are smooth functions of the thermodynamic temperature T. All these parameters are smooth functions of T_{90}, except for the discontinuity in the derivative $\mathrm{d}(T - T_{90})/\mathrm{d}T$ at T_{TPW}. Therefore uncertainties can be reduced and errors can be detected if the data on many, closely spaced isotherms are simultaneously fitted by physically motivated functions of T_{90} that have fewer parameters. For example, Moldover *et al* (1999) fitted six isotherms in the temperature range $217\,\mathrm{K} \leqslant T \leqslant 303\,\mathrm{K}$ independently with 24 parameters and then fitted the same data with surfaces that had either 11 or 12 parameters. With fewer parameters, the uncertainties of $T - T_{90}$ decreased. Smooth, physically based functions with few parameters can be generated by adding a simple analytic function (such as a polynomial function of $\log(T/\mathrm{K})$) to a theoretically based function (such as the second acoustic virial coefficient generated by Vogel *et al* (2010)) using an *ab initio* argon–argon potential).

Table 3 is adapted from table 9 of Pitre *et al* (2006) and from table 2 of Ripple *et al* (2007) to display the most important uncertainty components in these realizations of AGT. The tabulated values are the $k = 1$ components and their quadrature sum, expressed in parts per million of T.

Table 3 summarizes two realizations of AGT; each was the first to reach the listed highest or the lowest temperature. From the experience of these pioneering measurements, lower uncertainties may be possible in the future. For example, the helium used by Pitre *et al* might have contained either 2.5 ppm of neon or 1.1 ppm of argon (or some combination of neon and argon) that led to uncertainty contributions listed under 'Gas purity'. In future work, this contribution could be reduced by improved gas analysis and/or purification. In the work of Ripple *et al*, the uncertainty contributions listed under 'Microwave measurements' might be reduced by using a quasi-spherical cavity instead of a spherical cavity with incompletely resolved microwave triplets.

The uncertainties from 'Acoustic measurements' in table 3 resulted from inconsistencies in the values of $T - T_{90}$ obtained with different acoustic modes. At many temperatures, only a few acoustic modes could be used to determine $(T - T_{90})$ because the frequencies of the gas modes and shell modes were close together. This explains the somewhat surprising difference in the uncertainty of the 77.857 K and 77.657 K isotherms in table 3. In future thermometers, this uncertainty component might be reduced by increasing the ratio (shell thickness)/(cavity radius). At the lowest temperatures listed in table 3, the largest uncertainty contribution comes from the realization of T_{90}. In this range AGT is more accurate than realizations of the internationally accepted temperature scale.

12. Results from AGT

Figure 2 displays the values of $(T - T_{90})/T$ determined by various laboratories from AGT measurements published since 1990. The upper panel shows that these values fall outside the dotted curves representing the uncertainty of ITS-90 as estimated by Preston-Thomas *et al* (1990). In the upper panel, the dashed curve represents the function recommended by Working Group 4 (WG4) of the Consultative Committee for Thermometry for interpolating values of $(T - T_{90})/T$ between the fixed points (Fischer *et al* 2011). Working Group 4 determined this function using the plotted data together with both AGT data and non-AGT data at higher and lower temperatures than the data plotted.

The lower panel of figure 2 displays the deviations of the AGT data from WG4's function. The uncertainty bars represent one standard uncertainty, as claimed by the various authors. Between 119 K and 384 K, the standard deviation of the plotted points from WG4's function is 3.2×10^{-6}. This is a measure of the mutual consistency of realizations of AGT in diverse laboratories. These remarkably consistent results were

Table 3. Contributions to the $k = 1$ relative uncertainty of $10^6 \times (T - T_{90})/T$, determined by AGT, as implemented by Ripple *et al* (2007) and Pitre *et al* (2006).

T/K	Microwave measurements[a]	Thermostat and ITS-90 thermometry[b]	Acoustic measurements[c]	Gas purity	Gas properties[d]	Root sum of squares
Argon (Ripple et al 2007)						
552	1.7	0.8	3.1	0.7	0.5	3.8
550	1.7	0.8	3.0	0.7	0.5	3.6
470	1.3	1.1	1.6	0.4	0.4	2.3
466	1.3	1.1	1.4	0.4	0.4	2.4
394	1.2	0.9	1.3	0.5	0.3	2.0
367	1.1	1.0	1.1	0.5	0.3	1.9
364	1.1	1.0	1.1	0.5	0.3	1.9
333	1.0	1.1	0.8	0.0	0.3	1.8
Helium (Pitre et al 2006)						
234.31	0.9	0.6	1.3	1.5	0.0	2.2
192.08	0.8	0.8	2.1	1.5	0.0	2.9
161.39	0.9	1.1	1.9	1.5	0.0	2.7
127.55	0.9	1.4	6.0	1.5	0.0	6.4
96.41	1.1	1.2	1.5	1.5	0.0	2.7
83.801	1.2	1.1	6.4	1.4	0.0	6.8
77.857	0.9	1.2	3.6	1.4	0.0	4.1
77.657	0.9	1.2	2.2	1.4	0.0	3.0
24.551	3.7	7.7	2.0	1.4	7.7	11.8
19.679	2.5	8.1	4.1	1.4	9.6	13.7
13.837	4.3	10.1	2.9	1.4	10.1	15.2
10.293	5.8	11.7	1.0	1.4	7.7	15.5
7.0055	4.3	14.3	5.7	1.4	∼8	∼18

[a] Includes effects of: inconsistencies among modes, skin depth, antennas and transducers, and, only for Ripple *et al*, imperfect resolution of microwave triplets.
[b] Includes determination of T_{90} and temperature gradients.
[c] Includes inconsistencies among modes and uncertainty of thermal accommodation coefficient h.
[d] for argon, thermal conductivity; for helium, 3rd acoustic virial coefficient.

obtained using both helium and argon as thermometric gases in diverse cavity resonators. The cavities had radii ranging from 40 mm to 90 mm and their walls were made of either copper or aluminium, or stainless steel.

At 100 K and 90 K, the results from UCL and from INM-LNE diverge; however, the divergence is only slightly larger than the combined standard uncertainties. (Note: INM-LNE is now known as LNE-Cnam.) The cause of this divergence is not known. The divergence is too large to be explained by condensation of plausible concentrations of impurities in the thermometric gases. We suspect that the divergence is related to the approach to argon's triple point. For example, the term $A_3(T)\,p^3$ in equation (6) is not statistically significant; however, it might make a significant contribution $u^2(T,\ p)$ on to the 100 K and 90 K argon isotherms. (On the UCL argon isotherm at 90 K, u^2 decreases with pressure by 3%; on the INM-LNE helium isotherm at 84 K, u^2 increases 0.5%.) At these temperatures, the largest uncertainty component in $(T - T_{90})$ for both the UCL and INM-LNE measurements resulted from fitting the acoustic frequencies on the isotherms.

13. Prospects

13.1. High temperatures

We briefly consider the design parameters and problems that might be encountered in building an acoustic thermometer that operates at temperatures up to the freezing point of copper, $T_{Cu} = 1358$ K. The thermometric gas is likely to be argon because of its relative insensitivity to most impurities (section 9). The viscosity and thermal conductivity of argon are well known up to T_{Cu} (section 3.4). As discussed in section 6, the isothermal acoustic measurements could span the density range 40 mol m^{-3} to 200 mol m^{-3}, which corresponds to 450 kPa to 2.3 MPa. Because these pressures are 5 times larger than those encountered near T_{TPW}, the gas oscillations will drive the shell modes 5 times more strongly at T_{Cu} than at T_{TPW} and the frequency perturbations generated by the shell's recoil will be 5 times larger, all things being equal. (In equation (13), the prefactor is $\rho u^2 \approx (5/3)p$ and we ignore the decreasing compliances $G_{i,l}$ of the shell as the temperature increases.) This severe disadvantage can be reduced by increasing the ratio (thickness of shell) : (radius of cavity). Typically, measurements near T_{TPW} have used the ratio 1 : 5; a ratio of 1 : 2 (1 : 1) reduces the shell effect at low frequencies by a factor of 1.91 (2.62) and the breathing resonance frequency by 11% (24%). Because of the difficulty of thermostating large objects, the external dimensions of a high-temperature resonator will be similar to, or even smaller than, the dimensions of resonators used near T_{TPW}. Consequently, the cavity's radius will be reduced and the frequencies of the acoustic resonances will be higher at T_{Cu} than at T_{TPW} by a factor of at least 2.2 and possibly a factor of 4.

The ducts used by Ripple *et al* (2013) to conduct sound between the cavity and remote transducers at ambient

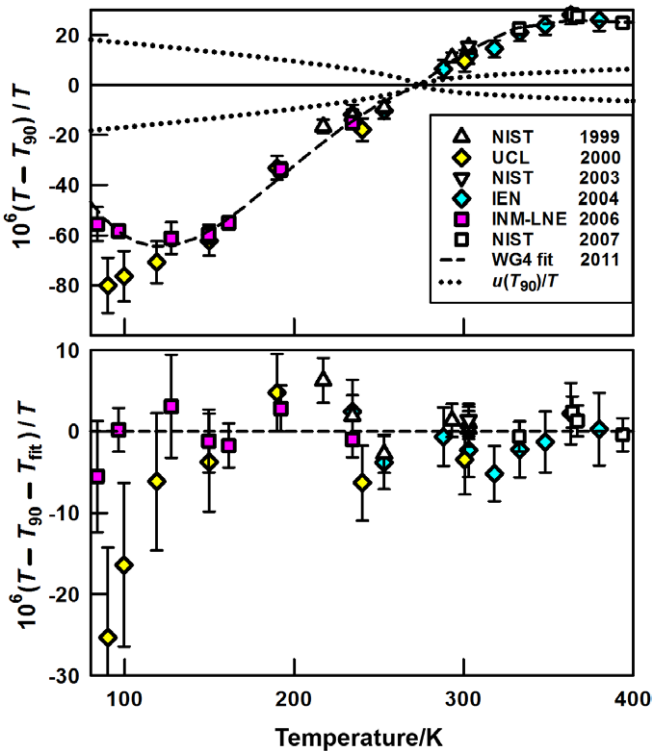

Figure 2. Top: values of $(T - T_{90})/T$ determined by AGT in various laboratories. The dotted curves represent the uncertainty $u(T_{90})$ from Preston-Thomas *et al* (1990). The dashed curve is Working Group 4's (WG4's) fit to the data shown and to other data (Fischer *et al* 2011). Bottom: the deviations of the plotted points from the fit by WG4. The plotted uncertainties are taken from the original publications which are for NIST, Moldover *et al* (1999), Strouse *et al* (2003) and Ripple *et al* (2007); for UCL, Ewing and Trusler (2000); for IEN, Benedetto *et al* (2004); for INM-LNE, Pitre *et al* (2006).

temperature will operate at T_{Cu}; however, Ripple's sound detector must be replaced by one that operates at higher frequencies. At constant density, smaller cavity radius reduces the Qs of the acoustic resonances as $(\text{radius})^{1/2}$; this is a minor disadvantage. The cavity's walls might be made of a Ni–Cr–Fe alloy chosen for its strength at T_{Cu}, resistance to oxidation, ease of fabrication, cost and availability in suitable forms (Feng *et al* 2013a). Feng *et al* demonstrated that silica-insulated coaxial cables can measure the microwave resonance frequencies of a cavity near T_{Cu}. Perhaps the greatest challenge to conducting AGT at T_{Cu} will be maintaining the purity of the argon. Because AGT is compatible with flowing gas, this challenge may be manageable.

13.2. Low temperatures

Pitre *et al* (2006) explored relative primary AGT in the temperature range 7 K to 25 K. Here, we address three problems that they encountered and the challenges of extending AGT down to the temperature of the λ-point of ^{4}He, $T_\lambda = 2.172$ K.

First, Pitre *et al* (2006) reported temperature 'noise' in the range 25 K to 77 K that was so large they could not measure $(T - T_{90})$ accurately. They traced the noise to a design flaw in their cryostat and they described how to avoid the problem in the future.

Second, Pitre *et al* (2006) reported that the acoustic resonances had large excess half-widths $\Delta g \equiv g_{meas} - g_{calc}$ when their cavity was filled with either helium at 4 K or argon at 95 K at 'high' gas densities. For these two isotherms, the values of Δg were so large that Pitre *et al* did not report values of $(T - T_{90})$. It is likely that the large values of Δg were caused by pre-condensation of the gas as its pressure approached the vapour pressure on these isotherms (Mehl and Moldover 1982). The effects of pre-condensation can be significantly reduced by either diamond turning or polishing the interior surfaces of the cavity. [The cavity used by Pitre *et al* (2006) had tooling marks from a conventional, numerically controlled milling machine.] In the future, pre-condensation will be detected, not only by its effects on Δg, but also by comparing the frequencies of TE and TM microwave modes measured while the gas is in the cavity (May *et al* 2004).

Third, Pitre *et al* (2006) generated sound in their cavity using a dc-biased capacitive microphone. At frequencies well below the resonance of the microphone's diaphragm, the acoustic pressure generated by the microphone was proportional to the product: $p_{ambient} \times Q_{acoustic}$. At constant density (and therefore approximately constant Q), the signal-to-noise ratio of the acoustic measurements was proportional to $p_{ambient}$ which itself was proportional to the temperature. Although Pitre *et al* did not discuss this problem, they solved it by increasing the densities (and therefore the Qs) spanned by their measurements at low temperatures. (At 273 K, their data ranged from 80 mol m^{-3} to 280 mol m^{-3}; at 7 K their data ranged from 140 mol m^{-3} to 390 mol m^{-3}.) Unfortunately, the acoustic frequencies at these higher densities and lower temperatures had significant contributions from the term $A_3(T)p^3$ in equation (6) and the uncertainty of this term was the largest contributor to the uncertainty of $(T - T_{90})$ in the range 7 K to 25 K.

For low-temperature measurements of $(T - T_{90})$, the signal-to-noise ratio could be increased by a factor of 10 to 30 by simply replacing a 6 mm diameter detector microphone with a 13 mm diameter microphone. The larger microphone will generate correspondingly larger perturbations to the acoustic frequencies; however, these perturbations will not cause significant problems because they are well understood and, like the elastic response of the cavity's walls, are proportional to the ambient pressure (Guianvarc'h *et al* 2009). Furthermore, the ambient pressures will be small in low-temperature AGT. Probably, an optimized measurement of $(T - T_{90})$ extending down to T_λ will use more than one cavity resonator. For example, one resonator could be optimized for the range T_{TPW} to 25 K and a second resonator could be optimized for the range 25 K to T_λ, where the ambient pressures will be a factor of ten lower.

Near T_λ the vapour pressure of ^{4}He is ∼5 kPa and the density of the saturated vapour is ∼280 mol m^{-3}. Under these conditions, we estimate the Q of the (0,2) acoustic mode is greater than 5000 for a cavity with a 50 mm radius. Thus, accurate AGT is possible unless pre-condensation is significant. An alternative gas for AGT is ^{3}He. At T_λ and 5 kPa, the Q for ^{3}He is approximately 1500 and the vapour pressure of ^{3}He is 27 kPa. Because of the higher vapour pressure, pre-condensation is less likely in ^{3}He than ^{4}He.

To summarize, accurate, primary, relative AGT appears to be possible between T_λ and T_{Cu}.

Acknowledgments

The authors thank Dean Ripple, Greg Strouse and Keith Gillis for their constructive comments on earlier drafts of this manuscript.

References

Barter C, Meisenheimer R G and Stevenson D P 1960 Diamagnetic susceptibilities of simple hydrocarbons and volatile hydrides *J. Phys. Chem.* **64** 1312

Benedetto G, Gavioso R M, Spagnolo R, Marcarino P and Merlone A 2004 Acoustic measurements of the thermodynamic temperature between the triple point of mercury and 380 K *Metrologia* **41** 74–98

Bruch L W and Weinhold F 2000 Diamagnetism of helium *J. Chem Phys.* **113** 8667–70

Cencek W, Komasa J and Szalewicz K 2011 Collision-induced dipole polarizability of helium dimer from explicitly correlated calculations *J. Chem. Phys.* **135** 014301

Cencek W, Przybytek M, Komasa J, Mehl J B, Jeziorski B and Szalewicz K 2012 Effects of adiabatic, relativistic, and quantum electrodynamics interactions on the pair potential and thermophysical properties of helium *J. Chem. Phys.* **136** 224303; see also supplementary material at http://dx.doi.org/10.1063/1.4712218 for tables of the thermophysical properties of helium

Cencek W, Garberoglio G, Harvey A H, McLinden M O and Szalewicz K 2013 Three-body nonadditive potential for argon with estimated uncertainties and third virial coefficient *J. Phys. Chem.* A **117** 7542–60

Chang R P and Abbott P J 2007 Factors affecting the reproducibility of the accommodation coefficient of the spinning rotor gauge *J. Vac. Sci. Technol.* A **25** 1567–76

Colclough A R, Quinn T J and Chandler T R D 1979 Acoustic redetermination of the gas-constant *Proc. R. Soc. Lond.* A **368** 125–39

Coppens A B and Sanders J V 1968 Finite-amplitude standing waves in rigid-walled tubes *J. Acoust. Soc. Am.* **43** 516–29

de Podesta M, Sutton G, Underwood R, Bell S, Stevens M, Byrne T and Josephs-Franks P 2011 Outgassing of water vapour, and its significance in experiments to determine the Boltzmann constant *Metrologia* **48** L1–6

de Podesta M, Sutton G, Underwood R, Perkin M, Davidson S and Morantz P 2011 Assessment of uncertainty in the determination of the Boltzmann constant by an acoustic technique *Int. J. Thermophys.* **32** 413–26

de Podesta M, Underwood R, Sutton G, Morantz P and Harris P 2013 Internal consistency in the determination of the Boltzmann constant using a quasispherical resonator *TEMPERATURE: Its Measurement and Control in Science and Industry* vol IX; *9th Int. Temperature Symp. (Anaheim, CA, 19–23 March 2012)* ed C W Meyer *AIP Conf. Proc.* **1552** 17–22 (New York: AIP)

de Podesta M, Underwood R, Sutton G, Morantz P, Harris P, Mark D F, Stuart F M, Vargha G and Machin G 2013 A low-uncertainty measurement of the Boltzmann constant *Metrologia* **50** 354–76

Edwards G and Underwood R 2011 The electromagnetic fields of a triaxial ellipsoid calculated by modal superposition *Metrologia* **48** 114–22

Ewing M B, McGlashan M L and Trusler J P M 1986 The temperature-jump effect and the theory of the thermal boundary layer for a spherical resonator. Speeds of sound in argon at 273.16 K *Metrologia* **22** 93–102

Ewing M B and Trusler J P M 2000 Primary acoustic thermometry between $T = 90$ K and $T = 300$ K *J. Chem. Thermodyn.* **32** 1229–55

Feng X, Gillis K A, Moldover M R and Mehl J B 2013a Microwave-cavity measurements for gas thermometry up to the copper point *Metrologia* **50** 219–26

Feng X J, Lin H and Zhang J T 2013b Temperature-jump effect for cylindrical resonators with low quality factors *TEMPERATURE: Its Measurement and Control in Science and Industry* vol IX; *9th Int. Temperature Symp. (Anaheim, CA, 19–23 March 2012)* ed C W Meyer *AIP Conf. Proc.* **1552** 34–8 (New York: AIP)

Fischer J, de Podesta M, Hill J D, Moldover M, Pitre L, Rusby R, Steur P, Tamura O, White R and Wolber L 2011 Present estimates of the differences between thermodynamic temperatures and the ITS-90 *Int. J. Thermophys.* **32** 12–25

Gammon B 1976 The velocity of sound with derived state properties in helium at −175 to 150 °C with pressure to 150 atm *J. Chem. Phys.* **64** 2556–68

Garberoglio G, Moldover M R and Harvey A H 2011 Improved first principles calculation of the third virial coefficient of helium *J. Res. Nat. Inst. Stand. Technol.* **116** 729–42

Gavioso R M, Benedetto G, Albo P A G, Ripa D M, Merlone A, Guianvarc'h C, Moro F and Cuccaro R 2010a A determination of the Boltzmann constant from speed of sound measurements in helium at a single thermodynamic state *Metrologia* **47** 387–409

Gavioso R M, Ripa D M, Guianvarc'h C, Benedetto G, Giuliano Albo P A G, Cuccaro R, Pitre L and Truong D 2010b Shell perturbations of an acoustic thermometer determined from speed of sound in gas mixtures *Int. J. Thermophys.* **31** 1739–48

Gavioso R M, Benedetto G, Ripa D M, Albo P A G, Guianvarc'h C, Merlone A, Pitre L, Truong D, Moro F and Cuccaro R 2011 Progress in INRiM experiment for the determination of the Boltzmann constant with a quasi-spherical resonator *Int. J. Thermophys.* **32** 1339–54

Gillis K A, Shinder I I and Moldover M R 2004 Thermoacoustic boundary layers near the liquid–vapor critical point *Phys. Rev.* E **70** 021201

Gillis K A and Moldover M R 1996 Practical determination of gas densities from the speed of sound using square-well potentials *Int. J. Thermophys.* **17** 1305–24

Gillis K A, Lin H and Moldover M R 2009 Perturbations from ducts on the modes of acoustic thermometers *J. Res. Nat. Inst. Stand. Technol.* **114** 263–85

Gillis K A 2012 Second-order boundary corrections to the radial acoustic eigenvalues for a spherical cavity *Metrologia* **49** L21–4

Greenspan M 1956 Propagation of sound in five monatomic gases *J. Acoust. Soc. Am.* **28** 644–8

Grimsrud D T and Werntz J H Jr 1967 Measurements of the velocity of sound in He^3 and He^4 gas at low temperatures with implications for the temperature scale *Phys. Rev.* **157** 181–90

Guianvarc'h C, Gavioso R M, Benedetto G, Pitre L and Bruneau M 2009 Characterization of condenser microphones under different environmental conditions for accurate speed of sound measurements with acoustic resonators *Rev. Sci. Instrum.* **80** 074901

Hamilton M F, Ilinskii Y A and Zabolotskaya E A 2001 Linear and nonlinear frequency shifts in acoustical resonators with varying cross sections *J. Acoust. Soc. Am.* **110** 109–19

Jäger B, Hellman R, Bich E and Vogel E 2011 Ab initio virial equation of state for argon using a new nonadditive three body potential *J. Chem. Phys.* **135** 084308

Jäger B 2013 Thermodynamic properties of gaseous argon from the *Ab Initio* virial equation of state *Z. Phys. Chem.* **227** 303–14

Lach G, Jeziorski B and Szalewicz K 2004 Radiative corrections to the polarizability of helium *Phys. Rev. Lett.* **92** 233001

Lin H, Feng X J, Gillis K A, Moldover M R, Zhang J T, Sun J P and Duan Y Y 2013 Improved determination of the Boltzmann constant using a single, fixed-length cylindrical cavity *Metrologia* **50** 417–32

Lin H, Gillis K A and Zhang J T 2010 Characterization of piezoelectric ceramic transducer for accurate speed-of-sound measurement *Int. J. Thermophys.* **31** 1234–47

Mark D F, Stuart F M and de Podesta M 2011 New high-precision measurements of the isotopic composition of atmospheric argon *Geochim. Cosmochim. Acta* **75** 7494–501

May E F, Moldover M R and Berg R F 2007 Reference viscosities of H_2, CH_4, Ar and Xe at low densities *Int. J. Thermophys.* **28** 1085–110

May E F, Pitre L, Mehl J B, Moldover M R and Schmidt J W 2004 Quasi-spherical resonators for metrology based on the relative dielectric permittivity of gases *Rev. Sci. Instrum.* **75** 3307–17

Mehl J B 2009 Second-order electromagnetic eigenfrequencies of a triaxial ellipsoid *Metrologia* **46** 554–9

Mehl J B 1985 Spherical acoustic resonator: effects of shell motion *J. Acoust. Soc. Am.* **78** 782–8

Mehl J B and Moldover M R 1982 Precondensation phenomena in acoustic measurements *J. Chem. Phys.* **77** 455–65

Mehl J B and Moldover M R 1986 Measurement of the ratio of the speed of sound to the speed of light *Phys. Rev.* A **34** 3341–4

Mehl J B, Moldover M R and Pitre L 2004 Designing quasi-spherical resonators for acoustic thermometry *Metrologia* **41** 295–304

Mehl J 2013 unpublished calculations

Moldover M R, Mehl J B and Greenspan M 1986 Gas-filled spherical resonators—theory and experiment *J. Acoust. Soc. Am.* **79** 253–72

Moldover M R, Trusler J P M, Edwards T J, Mehl J B and Davis R S 1988 Measurement of the universal gas constant *R* using a spherical acoustic resonator *J. Res. Natl Bur. Stand.* **93** 85–144

Moldover M R, Boyes S J, Meyer C W and Goodwin A R H 1999 Thermodynamic temperatures of the triple points of mercury and gallium and in the interval 217 K to 303 K *J. Res. Natl Inst. Stand. Technol.* **104** 11–46

Moldover M R 2009 Optimizing acoustic measurements of the Boltzmann constant *C. R. Physique* **10** 815–27

Mook W G (ed) 2000 *Environmental Isotopes in the Hydrological Cycle: Principles and Applications* (*UNESCO/IAEA Series on Environmental Isotopes in the Hydrological Cycle* vol 1) available online at: www.hydrology.nl/ihppublications/149-environmental-isotopes-in-the-hydrological-cycle-principles-and-applications.html

Olson J R and Swift G W 1996 Energy dissipation in oscillating flow through straight and coiled pipes *J. Acoust. Soc. Am.* **100** 2123–31

Patkowski K and Szalewicz K 2010 Argon pair potential at basis set and excitation limits *J. Chem. Phys.* **133** 094304

Patkowski K, private communication

Pitre L, Moldover M R and Tew W L 2006 Acoustic thermometry new results from 273 K to 77 K and progress towards 4 K *Metrologia* **43** 142–62

Pitre L, Sparasci F, Truong D, Guillou A, Risegari R and Himbert M E 2011 Measurement of the Boltzmann constant k_B using a quasi-spherical acoustic resonator *Int. J. Thermophys.* **32** 1825–86

Plumb H and Cataland G 1966 Acoustical thermometer and the National Bureau of Standards Provisional Temperature Scale 2–20 1965 *Metrologia* **2** 127–39

Podobedov B 2009 Resistive wall wakefields in the extreme anomalous skin effect regime *Phys. Rev. Spec. Top.—Accel. Beams* **12** 044401

Preston-Thomas H, Bloembergen P and Quinn T J 1990 *Supplementary Information for the International Temperature Scale of 1990* (BIPM: Sèvres) p 13; The 1997 reprint of this document is available at: www.bipm.org/utils/common/pdf/its-90/SInf_Foreword_and_Contents_2012.pdf

Ripple D C, Defibaugh D R, Moldover M R and Strouse G F 2003 Techniques for primary acoustic thermometry to 800 K *TEMPERATURE: Its Measurement and Control in Science and Industry* vol VII; *8th Int. Temperature Symp. (Chicago IL, 21–24 October 2002)* ed D C Ripple (New York: AIP) pp 25–30

Ripple D C, Strouse G F and Moldover M R 2007 Acoustic thermometry results from 271 K to 552 K *Int. J. Thermophys.* **28** 1789–99

Ripple D C, Murdock W E, Strouse G F, Gillis K A and Moldover M R 2013 Room temperature acoustic transducers for high-temperature thermometry *TEMPERATURE: Its Measurement and Control in Science and Industry* vol IX; *9th Int. Temperature Symp. (Anaheim, CA, 19–23 March 2012)* ed C W Meyer *AIP Conf. Proc.* **1552** 44–9 (New York: AIP)

Rizzo A, Hätttig C, Fernández B and Koch H 2002 The effect of intermolecular interactions on the electric properties of helium and argon: III. Quantum statistical calculations of the dielectric second virial coefficients *J. Chem. Phys.* **117** 2609–18

Schmidt J W and Moldover M R 2003 Dielectric permittivity of eight gases measured with cross capacitors *Int. J. Thermophys.* **24** 375–403

Song S and Yovanovich M M 1987 Correlation of thermal accommodation coefficient for engineering surfaces *National Heat Transfer Conf. (Pittsburgh, PA, 9–12 August 1987)*

Strouse G F, Defibaugh D R, Moldover M R and Ripple D C 2003 Progress in primary acoustic thermometry at NIST: 273 K to 505 K *TEMPERATURE: Its Measurement and Control in Science and Industry* vol VII; *8th Int. Temperature Symp. (Chicago IL, 21–24 October 2002)* ed D C Ripple (New York: AIP) pp 31–6

Tegeler Ch, Span R and Wagner W 1999 A new equation of state for argon covering the fluid region for temperatures from the melting line to 700 K at pressures up to 1000 MPa *J. Phys. Chem. Ref. Data* **28** 779–850, as implemented in the computer package: Lemmon E W, McLinden M O and Huber M L 2010 *REFPROP: Reference Fluid Thermodynamic and Transport Properties* NIST Standard Reference Database 23, Version 9.0 (Boulder, CO: National Institute of Standards and Technology) www.nist.gov/srd/nist23.cfm

Trusler J P M 1991 *Physical Acoustics and Metrology of Fluids* (New York: Taylor and Francis)

Underwood R J, Mehl J B, Pitre L, Edwards G, Sutton G and de Podesta M 2010 Waveguide effects on quasispherical microwave cavity resonators *Meas. Sci. Technol.* **21** 075103

Underwood R, Davidson S, Perkin M, Morantz P, Sutton G and de Podesta M 2012 Pyknometric volume measurement of a quasi-spherical resonator *Metrologia* **49** 245–56

Valkiers S, Vendelbo D, Berglund M and de Podesta M 2010 Preparation of argon primary measurement standards for the calibration of ion current ratios measured in argon *Int. J. Mass Spectrom.* **291** 41–7

Vogel E, Jäger B, Hellmann R and Bich E 2010 Ab initio pair potential energy curve for the argon atom pair and thermophysical properties for the dilute argon gas: II. Thermophysical properties for low-density argon *Mol. Phys.* **108** 3335–52

Zhang J T, Lin H, Sun X J, Feng K A, Gillis K A and Moldover M R 2010 Cylindrical acoustic resonator for the re-determination of the Boltzmann constant *Int. J. Thermophys.* **31** 1273–93

Zhang J T, Lin H, Feng X J, Sun J P, Gillis K A, Moldover M R and Duan Y Y 2011 Progress toward re-determining the Boltzmann constant with a fixed-path-length, cylindrical resonator *Int. J. Thermophys.* **32** 1297–329

Zhang J T, Lin H and Che J 2013 Effects of connecting tubing on a two-capillary viscometer *Metrologia* **50** 377–84

Supplement A: Calculated Corrections to Measured Acoustic Resonance Frequencies

The table below lists relationships used to calculate corrections to the measured acoustic resonance frequencies for a quasi-spherical cavity. This table was adapted from Benedetto *et al*. [1] with additions and corrections by Sutton [2] and new polynomial fits for the pair properties of argon [$B(T)$, $\beta(T)$, $\eta(T)$, $\lambda(T)$] from Mehl [3].

List of symbols

R	molar gas constant	ε_1, ε_2	Eccentricities of triaxial cavity
M	molar mass	r_{tr}	Radius of acoustic transducer
a	Average radius of quasi-spherical cavity	X_{tr}	Compliance/area of transducer
z_n	eigenvalue of n^{th} radial acoustic mode	λ_{sh}	Thermal conductivity of the shell
u_m	Speed of sound calculated from measured frequency	$C_{p,sh}$	Heat capacity of the shell

Notes to table below:

1. The polynomial fits to the properties of argon are only valid in the range: 180 K < T < 375 K. In a wider temperature range, the zero density properties of argon [$B(T)$, $\beta(T)$, $\eta(T)$, $\lambda(T)$] are tabulated in Supplement B of this document. In Ref. [1], the units for the virial coefficients of argon are in powers of "cm"; here, we use powers of "m"

2. The table includes additional relationships that are not present in Ref. [1] to provide a fuller explanation of the corrections.

Quantity	Unit	Relationship
2nd virial coefficient, argon	m^3mol^{-1}	$10^6 B\ T\ = 34.2004 - 11585T^{-1} - 962739T^{-2}$
3rd virial coefficient, argon	m^6mol^{-2}	use Eq. (21) from Jäger *et al*. (2011)
2nd acoustic virial coefficient, argon	m^3mol^{-1}	$10^6 \beta\ T\ = 62.732 - 11024.6T^{-1} - 1.2564 \times 10^6 T^{-2}$
Third acoustic virial coefficient,	m^6mol^{-2}	$\phi\ T\ = L - B\beta$ $L\ T\ = B + \left(2\gamma_0 - 1\right) T\frac{dB}{dT} + \left(\gamma_0 - 1\right) T^2 \frac{d^2B}{dT^2} \frac{\gamma_0 - 1}{\gamma_0} + \frac{1 + 2\gamma_0}{\gamma_0} C + \frac{\gamma_0^2 - 1}{\gamma_0} T\frac{dC}{dT} + \frac{\left(\gamma_0 - 1\right)^2}{2\gamma_0} T^2 \frac{d^2C}{dT^2}$
Speed of sound	$m\ s^{-1}$	$u\ p,T\ = \frac{RT\gamma_0}{M}\left(1 + \frac{\beta}{RT}\ p + \frac{\phi}{RT^2}\ p^2\right)^{0.5}$
Density	$kg\ m^{-3}$	$\rho\ p,T\ = \frac{-RT + \left(RT^2 + 4pBRT\right)^{0.5}}{2BRT} M$ Or, to order p^2,the molar volume is given by:

		$$V = \frac{RT}{p} + B + \frac{C - B^2}{RT} p$$ $$\rho\ p,T\ = \frac{M}{V}$$
Constant pressure heat capacity	J kg^{-1}K^{-1}	$$C_p\ p,T\ = \frac{5}{2}R - Tp\frac{d^2B}{dT^2}\ \frac{1}{M}$$ Or, to order p^2: $$X = \ B - T\frac{dB}{dT}\ ^2 - C + T\frac{dC}{dT} - \frac{T^2}{2}\frac{d^2C}{dT^2}$$ $$C_P\ p,T\ = \frac{5}{2}R - R\ \frac{T^2}{V}\frac{d^2B}{dT^2} - \frac{X}{V^2}\ \ \frac{1}{M}$$
Constant volume heat capacity	J kg^{-1}K^{-1}	$$C_v\ p,T\ = \frac{3}{2}R - R\ \frac{2T}{V}\frac{dB}{dT} + \frac{T^2}{V}\frac{d^2B}{dT^2} + \frac{T}{V^2}\frac{dC}{dT} + \frac{T^2}{2V^2}\frac{d^2C}{dT^2}\ \ \frac{1}{M}$$
Ratio of specific heat capacities		$$\gamma\ p,T\ = \frac{5}{3}\ 1 + 2\ \gamma - 1\ \frac{dB}{dT}\frac{p}{R} + \ \gamma - 1\ ^2T\frac{d^2B}{dT^2}\frac{p}{R}$$ Better to use ratio: $$\gamma\ p,T\ = \frac{C_P}{C_V}$$
Viscosity (argon)	Pa s	1) Viscosity in limit of zero pressure: $10^8\eta\ 0,T\ = 8.30585T - 1.14686 \times 10^{-5}T^3 + 1.105575 \times 10^{-8}T^4$ 2) Pressure virial: $b_T\ T\ = -1.185 \times 10^{-12}T^3 + 1.332 \times 10^{-9}T^2 - 5.253 \times 10^{-7}T + 7.698 \times 10^{-5}$ 3) Combine 1) and 2): $$\eta\ p,T\ = \eta\ 0,T\ \ 1 + b_T\ T\ \frac{p}{10^3}$$
Thermal conductivity (argon)	Wm^{-1}K^{-1}	$\lambda\ \rho,T\ = 6.47985 \times 10^{-5}T - 8.81693 \times 10^{-11}T^3 + 8.09179 \times 10^{-14}T^4 + 2.16 \times 10^{-5}\rho$
Thermal penetration length	m	$$\delta_{th}\ p,T\ = \frac{\lambda}{\pi\rho C_P f}^{0.5}$$
Viscous penetration length	m	$$\delta_v\ p,T\ = \frac{\eta}{\pi\rho f}^{0.5}$$
Thermal accommodation length for zero-density, monatomic gas	m	$$l_{th}\ p,T\ = \frac{\lambda}{p}\ \frac{\pi MT}{2R}^{0.5}\ \frac{2-h}{h}\ \frac{1}{2}$$
Thermal penetration length for shell (sh) material	m	$$\delta_{th,sh}\ p,T\ = \frac{\lambda_{sh}}{\pi\rho_{sh}C_{p,sh}f}^{0.5}$$

Thermal boundary layer correction (frequency) for a spherical cavity		$\frac{\Delta f_{th}\ p,T}{f_{0n}} = -\frac{\gamma-1}{2a}\delta_{th} + \frac{\gamma-1}{a} l_{th} + \frac{\gamma-1}{2a}\delta_{th,sh}\frac{\lambda_{gas}}{\lambda_{sh}}$ Radial modes only. Add to measured frequencies to get ideal frequency. The last term on the right hand side is small correction for thermal penetration into the shell of the resonator.
Contribution of thermal boundary layer to resonance half-width for a spherical cavity		$\frac{g\ p,T}{f_{0n}} = \frac{\gamma-1}{2a}\delta_{th} + \frac{\gamma-1}{2a}\delta_{th,sh}\frac{\lambda_{gas}}{\lambda_{sh}} - \frac{1}{2}\ \gamma-1\ \ 2\gamma-1\ \ \frac{\delta_{th}}{a}^{\ 2}$ Radial modes only. Last term on the right hand side is the second order thermal boundary layer correction of *Gillis* [4].
Contribution of bulk dissipation to resonance half-width		$\frac{g_{bd}\ p,T}{f_{0n}} = \frac{\pi^2}{u^2}\ \frac{4}{3}\delta_v^2 +\ \gamma-1\ \delta_{th}^2\ \ f^2$
Acoustic transducer perturbation for a spherical cavity		$\frac{\Delta f_{tr}}{f_{0n}} = -\frac{\rho u^2}{2}\frac{r_{tr}^2}{a^3}\mathrm{X}_{tr}$
Second order shape perturbation for a triaxial ellipsoid cavity		$\frac{dz_n^2}{z_n^2} = \frac{8z_n^2}{135}\ \epsilon_1^2 - \epsilon_1\epsilon_2 + \epsilon_2^2$ This is effectively a correction on u^2, not f
Calculate the speed of sound squared	m^2s^2	$u_m^2\ p,T\ = \ \frac{2\pi f_{0n}}{z_n}^{\ 2}\ a^2\ p,T$
Speed of sound squared corrected to the Triple point of water (TPW)		$u_m^2\ p,T_{TPW}\ = u_m^2\ p,T\ \ \frac{T_{TPW}}{T_{Sphere}}\ \ \frac{1+\frac{\beta\ T_{TPW}}{RT_{TPW}}p}{1+\frac{\beta\ T_{Sphere}}{RT_{Sphere}}p}$

[1] *Acoustic measurements of the thermodynamic temperature between the triple point of mercury and 380 K*, G Benedetto, R. M. Gavioso, R. Spagnolo, P. Marcarino and A. Merlone, *Metrologia* **41** (2004) 74-98.

[2] *Determination of the Boltzmann constant: acoustic models and corrections for argon and helium*, G Sutton, NPL Report ENG 19 (2009).

[3] *Supplement B*, J. B. Mehl, this document.

[4] *Second-order boundary corrections to the radial acoustic eigenvalues for a spherical cavity*, K. A. Gillis, *Metrologia* **49**, (2012) L21–L24.

Supplement B: Calculated Properties of Argon at Zero Density

The table below contains the properties of argon, calculated *ab initio* by James B. Mehl using the interaction potentials of Patkowski and Szalewicz [J Chem Phys 133, 094304 (2010)] and uncertainty code provided by Konrad Patkowski (private communication). That code accurately represents the numerical values of the potential within the uncertainty described in the paper.

The column headings are the temperature T, the second virial coefficient B, the second acoustic virial coefficient β_a, the viscosity η and the thermal conductivity λ, followed by estimates of the expanded (k = 2 corresponding to a 95 % confidence interval) uncertainties of the calculated quantities.

Linear interpolation of tabulated quantities is accurate to less than 0.3 of the corresponding uncertainties. However, cubic spline interpolation is recommended for better accuracy at intermediate temperatures. Cubic spline software is readily available in Fortran[1], C, Maple, Mathematica, MatLab, Octave, and spreadsheets.

The entries in the tabulated properties are formatted with more digits than are significant to avoid round-off errors in the interpolation.

At the end of the table, there are additional rows for the temperatures that are fixed points on the ITS-90. However, *all* of the tabulated values were calculated at the thermodynamic temperatures T. In principle, small corrections should be made to convert the tabulated values to ITS-90 values.

[1]In order to describe materials and procedures adequately, it is occasionally necessary to identify commercial products by manufacturer's name or label. In no instance does such identification imply endorsement by the National Institute of Standards and Technology, nor does it imply that the particular product or equipment is necessarily the best available for the purpose.

T K	B cm^3/mol	β_a cm^3/mol	η μPa s	λ mW K^{-1}m^{-1}	$U(B)$; k=2 cm^3/mol	$U(\beta_a)$; k=2 cm^3/mol	$U(\eta)$; k=2 μPa s	$U(\lambda)$; k=2 mW K^{-1}m^{-1}
80	-276.5519	-300.6960	6.56691	5.12691	1.68E+0	2.30E+0	6.21E-3	4.84E-3
82	-263.7753	-283.7193	6.72121	5.24723	1.59E+0	2.15E+0	6.39E-3	4.98E-3
84	-251.9541	-268.1949	6.87603	5.36795	1.51E+0	2.03E+0	6.58E-3	5.12E-3
86	-240.9877	-253.9499	7.03133	5.48905	1.44E+0	1.91E+0	6.75E-3	5.26E-3
88	-230.7890	-240.8346	7.18707	5.61051	1.37E+0	1.81E+0	6.93E-3	5.40E-3
90	-221.2820	-228.7215	7.34323	5.73230	1.31E+0	1.72E+0	7.10E-3	5.53E-3
92	-212.4003	-217.5019	7.49977	5.85439	1.26E+0	1.63E+0	7.26E-3	5.66E-3
94	-204.0855	-207.0821	7.65666	5.97676	1.21E+0	1.55E+0	7.43E-3	5.79E-3
96	-196.2862	-197.3810	7.81386	6.09938	1.16E+0	1.48E+0	7.58E-3	5.91E-3
98	-188.9570	-188.3261	7.97134	6.22223	1.11E+0	1.42E+0	7.73E-3	6.03E-3
100	-182.0574	-179.8555	8.12907	6.34528	1.07E+0	1.36E+0	7.88E-3	6.15E-3
105	-166.4617	-160.8964	8.52429	6.65362	9.81E-1	1.23E+0	8.23E-3	6.42E-3
110	-152.8710	-144.5793	8.92038	6.96268	9.04E-1	1.13E+0	8.55E-3	6.67E-3
115	-140.9281	-130.3913	9.31693	7.27211	8.37E-1	1.04E+0	8.83E-3	6.90E-3
120	-130.3550	-117.9412	9.71351	7.58160	7.80E-1	9.63E-1	9.09E-3	7.10E-3
125	-120.9323	-106.9285	10.10978	7.89087	7.29E-1	8.97E-1	9.32E-3	7.27E-3
130	-112.4847	-97.1228	10.50539	8.19964	6.85E-1	8.41E-1	9.51E-3	7.43E-3
135	-104.8704	-88.3342	10.90005	8.50770	6.46E-1	7.91E-1	9.68E-3	7.56E-3
140	-97.97370	-80.41043	11.29350	8.81483	6.11E-1	7.49E-1	9.82E-3	7.67E-3
145	-91.69919	-73.23489	11.68551	9.12086	5.80E-1	7.10E-1	9.94E-3	7.77E-3
150	-85.96751	-66.70573	12.07587	9.42562	5.52E-1	6.76E-1	1.00E-2	7.84E-3
155	-80.71216	-60.73979	12.46441	9.72899	5.26E-1	6.45E-1	1.01E-2	7.89E-3
160	-75.87701	-55.26808	12.85098	10.03084	5.03E-1	6.17E-1	1.01E-2	7.93E-3
165	-71.41436	-50.23198	13.23544	10.33107	4.82E-1	5.92E-1	1.02E-2	7.95E-3
170	-67.28341	-45.58262	13.61768	10.62959	4.63E-1	5.69E-1	1.02E-2	7.96E-3
175	-63.44910	-41.27743	13.99760	10.92634	4.45E-1	5.48E-1	1.02E-2	7.95E-3
180	-59.88110	-37.28012	14.37514	11.22124	4.29E-1	5.29E-1	1.01E-2	7.93E-3
185	-56.55304	-33.55968	14.75022	11.51426	4.14E-1	5.11E-1	1.01E-2	7.90E-3
190	-53.44193	-30.08834	15.12279	11.80535	4.00E-1	4.94E-1	1.00E-2	7.86E-3
195	-50.52758	-26.84260	15.49281	12.09447	3.87E-1	4.79E-1	9.93E-3	7.80E-3
200	-47.79225	-23.80108	15.86025	12.38162	3.74E-1	4.65E-1	9.85E-3	7.74E-3
205	-45.22023	-20.94690	16.22509	12.66676	3.63E-1	4.51E-1	9.75E-3	7.66E-3
210	-42.79761	-18.26301	16.58731	12.94990	3.52E-1	4.39E-1	9.64E-3	7.58E-3
215	-40.51198	-15.73491	16.94691	13.23102	3.42E-1	4.27E-1	9.52E-3	7.49E-3
220	-38.35228	-13.34933	17.30390	13.51012	3.33E-1	4.17E-1	9.39E-3	7.40E-3
225	-36.30860	-11.09546	17.65826	13.78721	3.24E-1	4.06E-1	9.25E-3	7.30E-3
230	-34.37204	-8.96287	18.01001	14.06229	3.16E-1	3.96E-1	9.11E-3	7.19E-3
235	-32.53457	-6.94214	18.35917	14.33537	3.08E-1	3.87E-1	8.96E-3	7.08E-3
240	-30.78895	-5.02664	18.70576	14.60647	3.01E-1	3.79E-1	8.81E-3	6.97E-3
245	-29.12863	-3.20653	19.04978	14.87561	2.94E-1	3.71E-1	8.65E-3	6.85E-3
250	-27.54765	-1.47569	19.39127	15.14279	2.87E-1	3.63E-1	8.49E-3	6.73E-3
260	-24.60254	1.74086	20.06676	15.67138	2.75E-1	3.49E-1	8.17E-3	6.48E-3
270	-21.91575	4.66778	20.73243	16.19242	2.63E-1	3.36E-1	7.84E-3	6.23E-3
280	-19.45557	7.33928	21.38854	16.70608	2.53E-1	3.24E-1	7.50E-3	5.98E-3
290	-17.19524	9.78655	22.03535	17.21256	2.44E-1	3.13E-1	7.18E-3	5.73E-3
300	-15.11205	12.03634	22.67312	17.71208	2.35E-1	3.03E-1	6.87E-3	5.49E-3
310	-13.18656	14.10805	23.30213	18.20483	2.27E-1	2.94E-1	6.58E-3	5.27E-3

320	-11.40207	16.02292	23.92266	18.69102	2.20E-1	2.85E-1	6.32E-3	5.06E-3
330	-9.74414	17.79666	24.53498	19.17086	2.13E-1	2.77E-1	6.09E-3	4.87E-3
340	-8.20022	19.44303	25.13935	19.64456	2.07E-1	2.70E-1	5.89E-3	4.71E-3
350	-6.75935	20.97453	25.73605	20.11231	2.01E-1	2.63E-1	5.74E-3	4.58E-3
360	-5.41194	22.40203	26.32533	20.57431	1.96E-1	2.57E-1	5.63E-3	4.48E-3
370	-4.14953	23.73509	26.90744	21.03075	1.90E-1	2.51E-1	5.58E-3	4.42E-3
380	-2.96464	24.98187	27.48262	21.48182	1.86E-1	2.45E-1	5.58E-3	4.40E-3
390	-1.85064	26.14988	28.05111	21.92769	1.81E-1	2.40E-1	5.62E-3	4.42E-3
400	-0.80163	27.24611	28.61313	22.36853	1.77E-1	2.35E-1	5.72E-3	4.48E-3
410	0.18766	28.27666	29.16891	22.80452	1.73E-1	2.30E-1	5.87E-3	4.57E-3
420	1.12195	29.24525	29.71865	23.23581	1.69E-1	2.26E-1	6.06E-3	4.69E-3
430	2.00548	30.15825	30.26255	23.66255	1.65E-1	2.21E-1	6.29E-3	4.85E-3
440	2.84207	31.01934	30.80080	24.08490	1.62E-1	2.17E-1	6.55E-3	5.04E-3
450	3.63517	31.83255	31.33360	24.50299	1.59E-1	2.14E-1	6.84E-3	5.24E-3
460	4.38792	32.60166	31.86111	24.91695	1.56E-1	2.10E-1	7.15E-3	5.47E-3
470	5.10313	33.32919	32.38351	25.32693	1.53E-1	2.06E-1	7.48E-3	5.72E-3
480	5.78339	34.01837	32.90095	25.73304	1.50E-1	2.03E-1	7.83E-3	5.98E-3
490	6.43106	34.67140	33.41361	26.13541	1.47E-1	2.00E-1	8.20E-3	6.25E-3
500	7.04827	35.29158	33.92161	26.53415	1.45E-1	1.97E-1	8.57E-3	6.53E-3
520	8.19903	36.44008	34.92426	27.32116	1.40E-1	1.91E-1	9.35E-3	7.12E-3
540	9.24955	37.47903	35.90996	28.09492	1.35E-1	1.86E-1	1.01E-2	7.73E-3
560	10.21154	38.42065	36.87969	28.85617	1.31E-1	1.81E-1	1.10E-2	8.35E-3
580	11.09501	39.27905	37.83438	29.60562	1.28E-1	1.78E-1	1.18E-2	8.98E-3
600	11.90851	40.05934	38.77484	30.34391	1.24E-1	1.73E-1	1.26E-2	9.61E-3
620	12.65944	40.77409	39.70184	31.07164	1.21E-1	1.67E-1	1.34E-2	1.02E-2
640	13.35418	41.42929	40.61608	31.78935	1.18E-1	1.64E-1	1.42E-2	1.09E-2
660	13.99831	42.03308	41.51822	32.49755	1.15E-1	1.61E-1	1.50E-2	1.15E-2
680	14.59668	42.57997	42.40886	33.19670	1.12E-1	1.60E-1	1.58E-2	1.21E-2
700	15.15359	43.08644	43.28856	33.88725	1.10E-1	1.54E-1	1.66E-2	1.27E-2
720	15.67279	43.54793	44.15783	34.56960	1.08E-1	1.52E-1	1.74E-2	1.33E-2
740	16.15762	43.98344	45.01715	35.24411	1.05E-1	1.49E-1	1.81E-2	1.39E-2
760	16.61104	44.37937	45.86697	35.91114	1.03E-1	1.51E-1	1.89E-2	1.45E-2
780	17.03569	44.74587	46.70770	36.57102	1.01E-1	1.45E-1	1.97E-2	1.51E-2
800	17.43393	45.08326	47.53973	37.22404	9.95E-2	1.43E-1	2.04E-2	1.57E-2
820	17.80787	45.39711	48.36343	37.87049	9.77E-2	1.40E-1	2.11E-2	1.63E-2
840	18.15941	45.68989	49.17912	38.51064	9.60E-2	1.39E-1	2.18E-2	1.68E-2
860	18.49026	45.95195	49.98714	39.14473	9.44E-2	1.33E-1	2.26E-2	1.74E-2
880	18.80197	46.20344	50.78776	39.77300	9.29E-2	1.34E-1	2.33E-2	1.79E-2
900	19.09593	46.43278	51.58128	40.39566	9.14E-2	1.37E-1	2.40E-2	1.85E-2
920	19.37342	46.63691	52.36796	41.01293	9.00E-2	1.32E-1	2.46E-2	1.90E-2
940	19.63559	46.84651	53.14804	41.62500	8.86E-2	1.28E-1	2.53E-2	1.96E-2
960	19.88349	47.03383	53.92175	42.23204	8.74E-2	1.28E-1	2.60E-2	2.01E-2
980	20.11810	47.19871	54.68932	42.83423	8.61E-2	1.25E-1	2.66E-2	2.06E-2
1000	20.34028	47.36080	55.45095	43.43175	8.49E-2	1.22E-1	2.73E-2	2.11E-2
1050	20.84652	47.69632	57.33030	44.90603	8.22E-2	1.18E-1	2.89E-2	2.24E-2
1100	21.29092	47.98526	59.17653	46.35417	7.97E-2	1.19E-1	3.05E-2	2.36E-2
1150	21.68239	48.23287	60.99208	47.77811	7.74E-2	1.14E-1	3.20E-2	2.48E-2
1200	22.02827	48.40390	62.77911	49.17956	7.53E-2	1.11E-1	3.35E-2	2.60E-2
1250	22.33466	48.55502	64.53955	50.56002	7.33E-2	1.07E-1	3.49E-2	2.71E-2
1300	22.60665	48.67981	66.27510	51.92085	7.15E-2	1.00E-1	3.63E-2	2.82E-2

1350	22.84853	48.77211	67.98729	53.26325	6.98E-2	1.04E-1	3.77E-2	2.93E-2
1400	23.06395	48.84186	69.67751	54.58833	6.83E-2	1.13E-1	3.91E-2	3.04E-2
1450	23.25600	48.87058	71.34701	55.89706	6.68E-2	9.58E-2	4.04E-2	3.14E-2
1500	23.42735	48.91386	72.99691	57.19034	6.55E-2	9.80E-2	4.17E-2	3.24E-2

83.810	-253.0365	-269.6085	6.86130	5.35646	1.52E+0	2.04E+0	6.56E-3	5.11E-3
161.406	-74.58637	-53.81020	12.95930	10.11543	4.97E-1	6.10E-1	1.01E-2	7.94E-3
234.320	-32.77889	-7.21126	18.31184	14.29835	3.09E-1	3.88E-1	8.98E-3	7.10E-3
273.160	-21.11519	5.53808	20.94078	16.35552	2.60E-1	3.32E-1	7.73E-3	6.15E-3
398.150	-0.99105	27.04840	28.50964	22.28735	1.78E-1	2.36E-1	5.70E-3	4.46E-3
302.910	-14.53625	12.65665	22.85705	17.85616	2.33E-1	3.00E-1	6.79E-3	5.43E-3
429.750	1.98398	30.13607	30.24902	23.65194	1.65E-1	2.21E-1	6.28E-3	4.85E-3
505.080	7.35079	35.59453	34.17795	26.73535	1.44E-1	1.95E-1	8.77E-3	6.68E-3
692.680	14.95433	42.90625	42.96783	33.63549	1.11E-1	1.56E-1	1.63E-2	1.25E-2
933.470	19.55161	46.77881	52.89405	41.42572	8.95E-2	1.29E-1	2.51E-2	1.94E-2
1234.930	22.24615	48.51552	64.01165	50.14607	7.40E-2	1.09E-1	3.45E-2	2.68E-2
1337.330	22.78987	48.75156	67.55555	52.92477	7.01E-2	1.02E-1	3.73E-2	2.90E-2
1357.770	22.88366	48.79080	68.25136	53.47028	7.00E-2	1.09E-1	3.79E-2	2.95E-2